Novel Optical Technique
for Real-Time Pattern/Image Recognition

by

Ying Qi

Thesis submitted to the faculty of
Virginia Polytechnic Institute and State University
in partial fulfillment of the requirements for the degree of

Master of Science
In
Electrical and Computer Engineering

Dr. Ting-Chung Poon, Chairman
Dr. Guy Indebetouw
Dr. Roger H. stolen

December 5, 2002

Blacksburg, Virginia

Keywords: optical pattern recognition, JTC, two-pupil heterodyne, SLM.

Novel Optical Technique
for Real-Time Pattern/Image Recognition

By

Ying Qi

Ting-Chung Poon, Chairman

Electrical and Computer Engineering

(Abstract)

We propose a novel real-time joint-Transform correlation (JTC) technique for optical pattern recognition.

To replace the film recording aspect of performing optical correlation, conventional real-time joint-Transform correlation (JTC) optical systems make use of a spatial light modulator (SLM) located in the Fourier plane to record the interference intensity to achieve real-time processing. However, the use of a SLM in the Fourier plane, is a major drawback in these systems since SLMs are limited in resolution, phase uniformity and contrast ratio. Thus, they are not desirable for robust applications. In this thesis, we developed a hybrid (optical/electronic) processing technique to achieve real-time joint-Transform correlation (JTC). The technique employs acousto-optic heterodyning scanning. The proposed real-time JTC system does not require a SLM in the Fourier plane as in conventional real-time JTC systems. This departure from the conventional scheme is extremely important, as the proposed approach does not depend on SLM issues. We have developed the theory of the technique and substantiated it with optical experimental as well as computer simulation results.

Acknowledgments

I would first like to express my sincere appreciation to my advisor, **Dr. Ting-Chung Poon,** for his insightful guidance, comments, patience, encouragement, understanding and support throughout my research work, and giving me this opportunity to study with him.

Special thanks are due to **Dr. Guy J. Indebetouw** for supplying some of the patterns used in the experiment and serving on the advisory committee, and to **Dr. Roger Stolen** for being my instructor for two semesters and serving on the advisory committee.

I also thank my fellow students at the Optical Image Processing Laboratory at Virginia Tech for all their help and advice. Special thanks are given to Bill Yoder, who helped me throughout my research study: I wish him good luck in his graduate study.

Finally, I give my sincere love and thanks to my dear husband, for his love, caring, and understanding. I thank my whole family for their endless love.

We want to express our gratitude for the financial support by the National Science Foundation (ECS-9810158).

Table of contents

List of Figures:

Chapter 1 Introduction

Optical pattern recognition is one of the most powerful operations possible on a coherent or an incoherent optical system. Matching two images and learning the likelihood of two pattern-matched objects are one of the main roles in various schemes of pattern recognition operations [1]. In the application of optical pattern recognition, correlation peaks are generally used for detection of signal and, therefore, to distinguish the difference between the reference object and the target object. With the potential application in military, biology, robot navigation and other areas, various methods for optical pattern recognition have been proposed and rejuvenated over the past decades.

In optical correlation systems, there are two commonly used techniques available in practice: one is to utilize the holographic matched filter technique, and the other is to utilize the joint-transform correlation method. In matched filtering, a wide variety of filters, such as Vander Lugt, phase-only, binary phase, etc., have been proposed for different requirements. The joint transform correlation (JTC) was first proposed by Weaver and Goodman in the 1960's and is a major subject in many current optical pattern recognition systems [2]. It can be easily realized with the advent of spatial light modulators (SLMs). In the JTC, a reference pattern and a target pattern are placed side by side in the front focal plane of a lens. The lens performs a Fourier transform of the two patterns and produces a Fourier transform interference pattern, or the so called joint-power spectrum on the back focal plane (output plane) of the lens. This joint power spectrum can be recorded electronically in a SLM or some other holographic material devices for real-time display. A "reading" laser beam can then be used to diffract from this interference pattern and produce a signal corresponding to the optical correlation between the reference pattern and the target pattern. One significant advantage of a JTC system over the matched filter-based correlator is that the JTC system does not require the computation of a new filter function every time the reference pattern changes. Also, JTC systems are less sensitive to optical system alignment than a filter-based system and the reference pattern can be updated in real time. With the advanced development of

modern technology, the joint transform correlation has been developed heading several directions with different devices [3,4,5,6,7].

One typical modern real-time JTC system is to utilize a spatial light modulator (SLM) in the Fourier plane to store the interference intensity, which is subsequently read out by the coherent light. The systems using SLMs are extremely flexible in that changing the reference pattern for the system merely involves changing the pattern at the system reference plane [8,9,10]. However, it has been pointed out that there are some limitations by using SLMs. One critical problem is that the SLMs will be very expensive to satisfy the high-resolution requirement for recording of the image transform. Also, the effect produced in a correlation by an aberration in the optical JTC system has been experimentally observed such that correlation is lost to a great extent if there is not an adequate control of the optical system parameters. For example, a little de-focusing error on the Fourier plane can produce a significant loss of the correlation signal. Other problems come from the design considerations such as phase uniformity and contrast ratio of SLMs [11,12].

The use of a magneto-optic device (MOD) with a liquid crystal light valve (LCTV) are employed in other real-time JTC systems with the input object functions written into the MOD by a programmable computer, and the corresponding power spectral distribution read out coherently by a LCTV for correlation operation. But this type of system also suffers with low SNR and high cost [2].

Since the correlation of two images is also one of the mathematical operations in image processing and pattern recognition systems, a digital computer has been considered as an alternative way to realize pattern recognition. But as the images become more and more complex and large in size, the calculation becomes more and more time consuming for the digital computer for the high-resolution requirement. Therefore, optical processing may still be the alternative way for digital processing because it offers greater speed.

To overcome the drawbacks of using SLM (such as the use of CCD camera or LCTV) in the Fourier plane, some also consider scanning optical processing which is fast, accurate and flexible. In this thesis, under the theory of 2-D pattern recognition, we combine a scanning optical technique with electronic processing to achieve real-time joint-transform correlation for pattern recognition purposes without using any SLM in the

Fourier plane. The system is hybrid (optical/electronic) in nature and its advantage is that the speed and data acquisition rate of such a hybrid optical-electronic processing can be made compatible with that of subsequent digital or optical signal processing. This thesis is divided into 4 chapters that are outlined as follows.

Chapter 2 will present a general theory of the hybrid optical system, which employs the theory of optical heterodyne scanning for real-time optical pattern recognition. The corresponding experimental results are also available in this chapter.

In section 2.1, we will briefly overview the standard structure of a real-time joint-Transform correlation system under the use of SLM in the system, which gives the basic knowledge about optical correlation and realization. The limitations of using SLM also will be discussed in detail. Section 2.2 will be devoted to the introduction of the two-pupil heterodyne scanning system with the use of an acousto-optic modulator operating at the Bragg regime. The system will produce a heterodyne current at the output, and the information carried by the current is characterized by the amplitude and the phase. Also, most of the conceptions, notations and symbols will be defined in these two sections and will be used throughout the thesis. Section 2.3 will show that when a chirped grating is used and optically scanned, we can perform the cross-correlation of two patterns without the major drawbacks encountered in conventional real-time JTC systems. In the system, x-scanner denoted by $x=x(t)$ is used to represent the instantaneous position of the scanning pattern; 1-D scanning chirped grating is characterized by $|T_0|^2 = 1+\cos(ax^2)$, which will result in the correlation of the two pupils presented in the system and thus realize real-time correlation. In section 2.4, we will develop the optical system in the context of joint-transform correlation without using any SLMs in the focal plane, and describe an electronic extraction scheme to display the correlation information. Finally, the standard for optical pattern recognition using our proposed system is theoretically verified. A practical optical implementation of the proposed hybrid (optical/electrical) system is then demonstrated and described in section 2.5. By performing the proposed real-time JTC system shown in section 2.5, experimental results with different reference and target patterns are presented in section 2.6. A basis for the potential applications of real-time optical pattern recognition, for example, fingerprint identification, is well

developed. Section 2.7 will give a detailed analysis of the experimental correlation results provided in section 2.6, and the results will be discussed.

To further effectively verify and reinforce our proposed optical pattern recognition technique based on optical heterodyne scanning, computer simulations have been done by developing the Matlab program. To make an easy comparison, the computer simulation results are displayed in the same order as the experimental results. Details about computer simulation will be shown in chapter 3.

In chapter 4, we will present a summary of this thesis and give some concluding remarks. Future research work is also considered and listed in this final chapter.

Chapter 2 Optical Pattern Recognition System

The goal pursued in this chapter is to present a novel real-time optical technique using acousto-optic (AO) two-pupil heterodyning system for optical pattern recognition. The conventional real-time joint-Transform correlation (JTC) system is first introduced and some of its major drawbacks are pointed out. We then present a practical optical implementation of an optical/electronic hybrid system based on AO two-pupil heterodyning without the major drawbacks, which is encountered in conventional systems. Experimental results are demonstrated and fully discussed.

First, the standard architecture of a joint-Transform correlation (JTC) system is reviewed in section 2.1. Next, the theory of the two-pupil optical heterodyning system is provided in section 2.2, and corresponding real-time correlation realization and real-time JTC without using SLM in the focal plane are given in section 2.3 and section 2.4. In section 2.5, a practical implementation of the idea for optical pattern recognition is provided. Section 2.6 gives the experimental results for real-time pattern recognition. Finally, further discussion of the results is given in section 2.7.

2.1 Standard Structure of joint-Transform Correlation (JTC) System

Optical correlators are generally divided into two types depending upon the techniques: the matched spatial filtering optical correlator, and the joint-transform correlator. The joint-transform correlator has good characteristics for real-time pattern recognition because of easy adjustment of the optics without preparing complicated matched spatial filters. In this thesis, we develop a novel joint transform correlator.

The standard architecture of a joint-Fourier transform correlator is a two-stage system [13]. In the first stage, the reference object and the target object are directly written on a spatial light modulator (SLM), and subsequently, in the second stage, the detection of the so-called Joint-Fourier Transform power spectrum is performed by another spatial light modulator which may be coherently read out for correlation operation. Figure 1 shows a conventional real-time JTC system, where the reference object is denoted as $g_1(x-x_0, y)$ and the target object is denoted as $g_2(x+x_0, y)$. The joint-transform power spectrum, $P(k_x, k_y)$, on the back of the focal plane of lens L_1 is given by

$$\begin{aligned} P(k_x,k_y) &= \left|F\{g_1(x-x_0,y)\}+F\{g_2(x+x_0,y)\}\right|^2 = \left|G_1(k_{x,}k_y)\right|^2+\left|G_2(k_{x,}k_y)\right|^2 \\ &+G_1^{*}(k_x,k_y)G_2(k_{x,}k_y)\exp(j2k_xx_0)+G_1(k_x,k_y)G_2^{*}(k_{x,}k_y)\exp(-j2k_xx_0), \end{aligned} \tag{1}$$

where $G_i(\frac{k_0x}{f},\frac{k_0y}{f})$ is the Fourier transform of the function $g_i(x, y)$ for i=1,2, and is given by

$$G_i(k_x,k_y)=\iint g_i(x,y)\exp[j(k_xx+k_yy)]dxdy = F\{g_i(x,y)\}_{k_x,k_y} \tag{2}$$

with $k_x=k_0x/f$ and k_0y/f, where f is the focal length of Lens L_1 and k_0 is the wave number of the laser. In real-time JTC systems, the joint-Transform power spectrum is detected by a spatial light modulator (SLM) or a CCD camera. The output of the CCD camera is fed to another spatial light modulator for coherent display as illustrated in Fig.1, where lens L_2 is a Fourier transform lens with the same focal length as lens L_1. Due to the coherent display on the correlation plane we have the Fourier transform of P (k_x, k_y) as follows:

$$F\left\{P(\frac{k_0x}{f},\frac{k_0y}{f})\right\}_{k_x,k_y} = A_{11}(-x,-y)+A_{22}(-x,-y)+A_{12}(-x-2x_0,-y)+A_{21}(-x+2x_0,-y), \tag{3}$$

Where $A_{ij}(x,y)=g_i(x,y)\otimes g_j(x,y)=\iint g_i^{*}(x',y')g_j(x+x',y+y')dx'dy'$ (4)

with $i=1$ or 2, and $j=1$ or 2. The symbol $\otimes$ denotes correlation involving coordinates x and y. $A_{ij}(x,y)$ is the autocorrelation when $i=j$, and is the cross-correlation when $i \neq j$. Hence, if the target and the reference objects are the same, besides a strong peak at the origin of the correlation plane due to the first two terms of equation (3), we have two strong peaks centered at $x=\pm 2x_0$ due to the last two terms in (3).

The advantage of using the JTC technique is that the input images are Fourier transformed simultaneously, so the interference among the transforms is achieved in a single step, other advantages of JTC are that the reference images can be updated in real time and the problem of accurate optical alignment of filter occurring with matched filtering is significantly reduced [4]. However, there are two major drawbacks with this conventional real-time system. Owing to the existence of zero-order spectra, i.e., the first two terms in equation (1), a physical separation between the reference object and the target object is required [14]. This requirement hampers the utilization efficiency of the input spatial domain and lowers the diffraction efficiency of the correlation peaks, and attempts have been made to alleviate this problem [15-23]. Another major drawback is the requirement of high spatial resolution of the SLM for coherent display. From the last two terms in equation (1), we see that

$$G_1^*(k_x,k_y)G_2(k_x,k_y)\exp(j2k_x x_0)+G_1(k_x,k_y)G_2^*(k_x,k_y)\exp(-j2k_x x_0)= 2\left|G_1(k_x,k_y)G_2(k_x,k_y)\right|\cos(2k_x x_0+\theta), \tag{5}$$

where θ is the phase angle of $G_1^* G_2$. We see that the correlation information is carried by a spatial carrier with frequency $2x_0/\lambda f$, where $\lambda=2\pi/k_0$, is the wavelength of light, and we have made use of $k_x=k_0 x/f$ into the argument of cosine term to find the frequency of the spatial carrier. Now let us give an example. For $2x_0=30mm$, $\lambda=0.6um$, and $f=50cm$, the required spatial resolution of the SLM is $2x_0/\lambda f \sim$ 100cycle/mm. Very often in practice, $2x_0$ is made to be small enough or the focal length f is made large enough so that the CCD camera or the subsequent SLM can resolve the spatial carrier. Hence, the spatial resolution requirement of the CCD and SLM should be generally high enough, i.e., the CCD camera and the subsequent SLM must be able to resolve the fine details in order to have the real-time system work. In addition, phase uniformity and contrast ratio of the SLM also are important considerations.

In order to avoid the major drawbacks of using SLMs, we proposed a hybrid optical/electronic system that can perform real-time correlation without these critical drawbacks. Specifically, there is no need to place a SLM at the Fourier plane to detect the Joint-Fourier power spectrum and the use of another SLM for coherent display. The corresponding optical heterodyne scanning theory and practical optical implementation are introduced in section 2.2 and section 2.3.

IN comparison to the conventional real-time JTC system described above, the novel real-time JTC system we proposed overcomes the two major drawbacks: First, by using a two-pupil optical heterodyning system, the zero-order spectrum (auto-correlation item) becomes a constant added with the cross-correlation item (see equation (22)), and can be removed easily. Second, in the proposed system, the cross-correlation results are transferred to the time domain by using scanning. So, no high spatial resolution spatial light modulators are needed. While our system overcomes the major drawbacks of a conventional JTC system, it maintains the major advantage of being real-time.

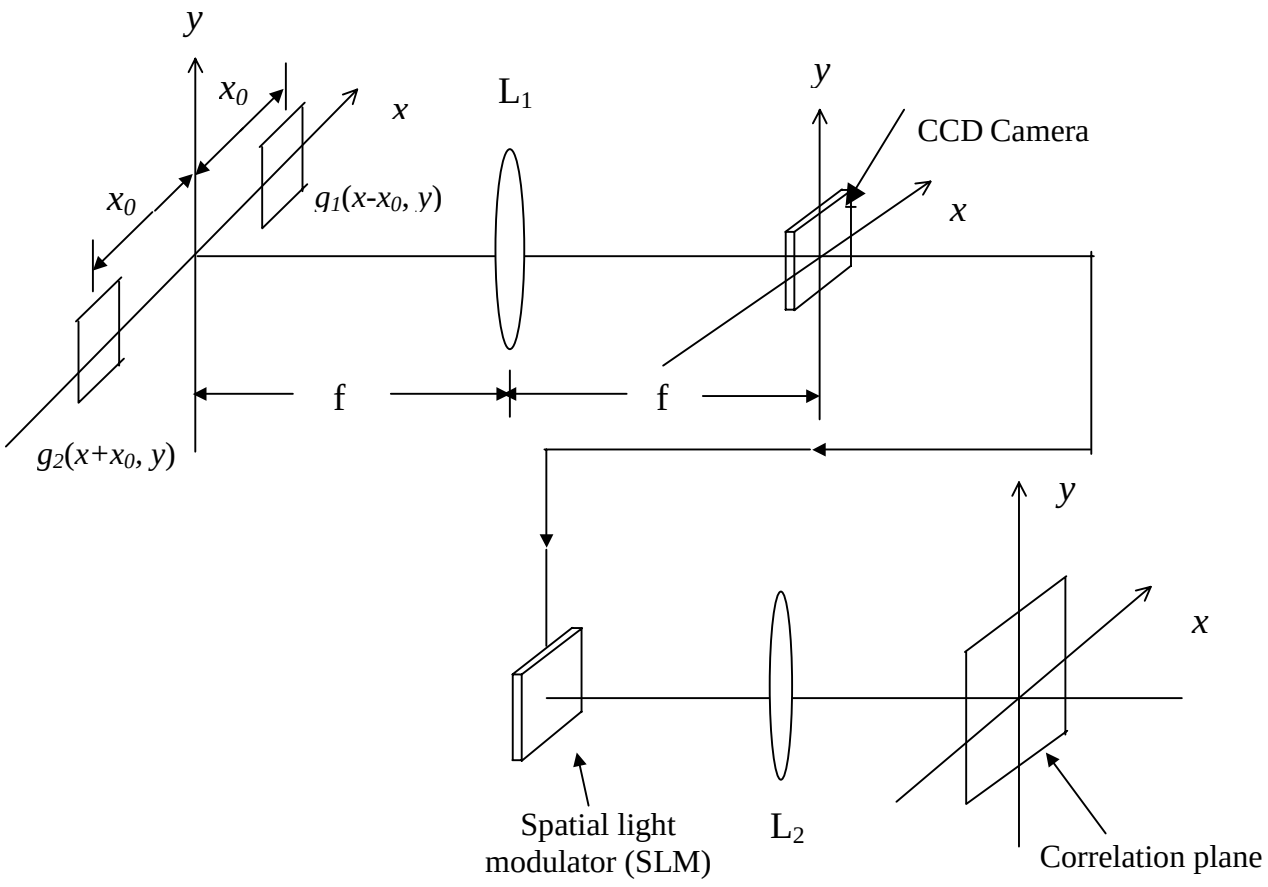

Figure. 1 Conventional real-time Joint-Transform correlation (JTC) system

2.2 Basic Knowledge of Two-pupil Optical Heterodyning System: Introduction and Background

In order to establish a good foundation for understanding the practical optical system set up, we will briefly review the theory of two-pupil optical heterodyne scanning, which was first developed by Poon and Korpel [24]. The so-called two-pupil optical heterodyne scanning system involves acousto-optic frequency shifting and heterodyne detection. We shall call the system a two-pupil acousto-optic heterodyning system [25]. Such a processor is brought about by acousto-optic Bragg diffraction, and the output of the system is a heterodyne radio frequency (RF) current.

An idealized scheme of a two-pupil heterodyning image processing system is shown in figure 2.

In this system, a transparency function $p_1(x, y)$, is located at the front focal plane of lens L with a focal length f, the other transparency function $p_2(x, y)$ is also located at the same focal plane as function $p_1(x, y)$ is. The transparency functions $p_1(x, y)$ and $p_2(x, y)$ are usually called the pupil functions [25]. A collimated laser beam at temporal frequency ω_0 is used to illuminate pupil function $p_1(x, y)$, the other pupil function $p_2(x, y)$ is illuminated by a laser beam with different temporal frequency $\omega_0 + \Omega$. The laser's temporal frequency offset of Ω can be realized by an acousto-optical modulator (AOM). The two pupil functions are focused into the back focal plane of lens L, where lens L forms the 2-D Fourier transform $P_1(k_0 x/x, k_0 y/f)$, and $P_2(k_0 x/f, k_0 y/f)$ of $p_1(x, y)$, and $p_2(x, y)$, respectively, in its back focal plane.

The combined optical scanning field on the back focal plane is given by the following equation:

$$P\left(\frac{k_0 x}{f}, \frac{k_0 y}{f}\right) exp(j\omega_0 t) + P_2\left(\frac{k_0 x}{f}, \frac{k_0 y}{f}\right) exp[j(\omega_0 + \Omega)t], \tag{6}$$

where $P_i\left(\frac{k_0 x}{f}, \frac{k_0 y}{f}\right) = F\{p_i(x, y)\}_{\frac{k_0 x}{f}, \frac{k_0 y}{f}}$ and $i = 1, 2$, The combined optical field or the scanning pattern is used to 2-D raster scan a target with amplitude distribution given by $T_0(x, y)$ located on the back focal plane of lens L. Alternatively, the target can be placed on a x-y scanner platform, as shown in Figure.2, while the optical beam is stationary. The

photo-detector, which responds to the intensity of the optical transmitted field or scattered field, will collect all the light and delivers a current i (x, y) which is given by

$$i(x,y)=\iint_A \left|\{P_1(\frac{k_0x'}{f},\frac{k_0y'}{f})exp(j\omega_0t)+P_2(\frac{k_0x'}{f},\frac{k_0y'}{f})exp[j(\omega_0+\Omega)t)]\}\right.$$
$$\left.\times T_0(x+x',y+y')\right|^2 dx'\,dy', \tag{7}$$

We will point out that the integration is over the area A of the photo-detector. *x=x(t)* and *y=y(t)* represent the instantaneous position of the scanning pattern, and the shifted coordinates of T_0 represents the movement of scanning. For the content of the current, we point out that the current out of the photo-detector includes the base-band current and the RF heterodyne current at the temporal frequency Ω. What we are interested in is the heterodyne current as it contains the useful information and is given by:

$$i_\Omega(x,y)=Re[\iint_A P_1^*(\frac{k_0x'}{f},\frac{k_0y'}{f})P_2(\frac{k_0x'}{f},\frac{k_0y'}{f})|T_0(x+x',y+y')|^2\,dx'\,dy'\,exp(j\Omega t)]. \tag{8}$$

Note that we have used the convention for phasor ψ_p as $\Psi(x,y,t)=Re[\Psi_p(x,y,t)exp(j\Omega t)]$, Where Re [.] denotes the real part.

Now equation (8) can be written as:

$$i_\Omega(x,y)=Re[i_{\Omega p}(x,y)exp(j\Omega t)], \tag{9}$$

where

$$i_{\Omega p}(x,y)=\iint_A P_1^*(\frac{k_0x'}{f},\frac{k_0y'}{f})P_2(\frac{k_0x'}{f},\frac{k_0y'}{f})|T_0(x+x',y+y')|^2\,dx'\,dy'\ . \tag{10}$$

Equation (10) denotes the output phasor, which includes the amplitude and the phase information of the heterodyne current. The phasor constitutes the scanned and processed version of the target $|T_0|^2$ [24,26]. From this point we can see that this optical scanning system can process intensity distribution of the object being scanned under certain conditions. This system has been used for 3-D holography, 3-D fluorescence microscopy, bipolar incoherent image processing and some other image processing at Virginia Tech's Optical Information Processing Lab [26]. Using this knowledge, with some modifications, we employ this so-called two-pupil heterodyne scanning technique to perform real-time correlation, which will be introduced in the following section.

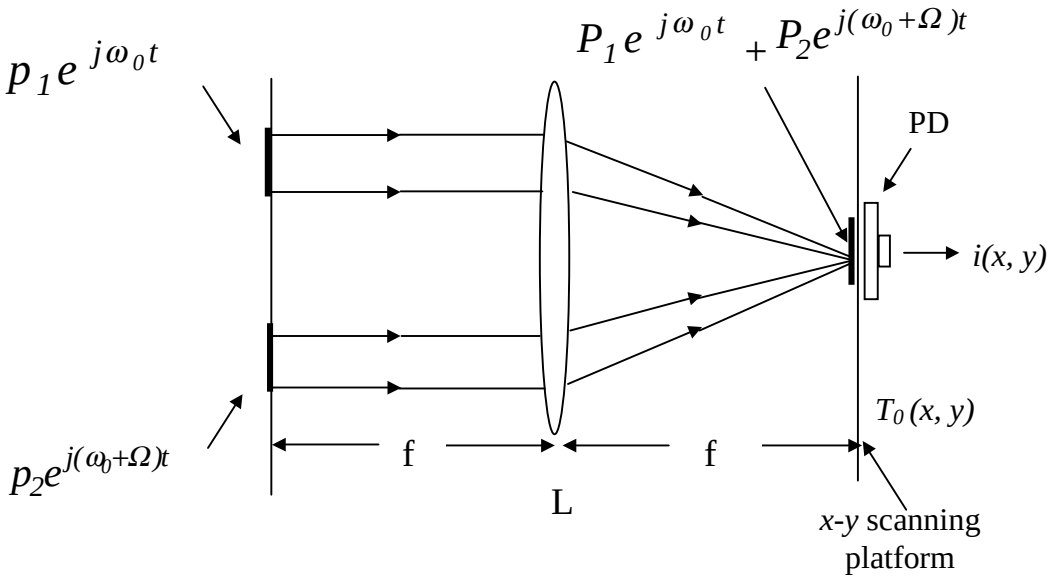

Figure. 2 Idealized optical heterodyne scanning system

2.3 Corresponding Real-Time Correlation Realization

Based upon the theory presented in section 2.2, we are able to perform 1-D scanning of a chirped grating which will result in the correlation of the two pupil functions (one is for the reference object, and the other is for the target object) introduced in our optical heterodyne scanning system.

In order to show the real-time correlation, we let $|T_0|^2 = 1 + cos(ax^2)$, where a is a grating constant, since $cos(ax^2) = \frac{1}{2}[exp(jax^2) + exp(-jax^2)]$, equation (10) can be written as:

$$
\begin{aligned}
& i_{\Omega_p}(x) = \iint_A P_1^*\left(\frac{k_0 x'}{f}, \frac{k_0 y'}{f}\right) P_2\left(\frac{k_0 x'}{f}, \frac{k_0 y'}{f}\right) \times \\
& \{1 + \frac{1}{2} exp[(ja(x + x')^2 + \frac{1}{2} exp[(-ja(x + x')^2]\} dx'\, dy' \\
& = I_0 + \frac{1}{2} t_1(x) + \frac{1}{2} t_2(x),
\end{aligned}
\tag{11}
$$

where $I_0 = \iint_A P_1^*\left(\frac{k_0 x'}{f}, \frac{k_0 y'}{f}\right) P_2\left(\frac{k_0 x'}{f}, \frac{k_0 y'}{f}\right) dx'\, dy'$, (12)

$$
t_1(x) = \iint_A P_1^*\left(\frac{k_0 x'}{f}, \frac{k_0 y'}{f}\right) P_2\left(\frac{k_0 x'}{f}, \frac{k_0 y'}{f}\right) exp[ja(x + x')^2]\, dx'\, dy', \tag{13}
$$

and

$$
t_2(x) = \iint_A P_1^*\left(\frac{k_0 x'}{f}, \frac{k_0 y'}{f}\right) P_2\left(\frac{k_0 x'}{f}, \frac{k_0 y'}{f}\right) exp[-ja(x + x')]^2\, dx'\, dy'. \tag{14}
$$

We can see that the first term I_0 is some complex constant. What we are really interested in is the second and the third term given by equations (13) and (14). By expanding the exponential term and re-arranging, equation (13) can become:

$$
\begin{aligned}
& t_1(x) = exp(jax^2) \iint_A P_1^*\left(\frac{k_0 x'}{f}, \frac{k_0 y'}{f}\right) P_2\left(\frac{k_0 x'}{f}, \frac{k_0 y'}{f}\right) exp(jax'^2)\, exp(j2axx')\, dx'\, dy' \\
& = exp(jax^2) F\{P_1^*\left(\frac{k_0 x}{f}, \frac{k_0 y}{f}\right) P_2\left(\frac{k_0 x}{f}, \frac{k_0 y}{f}\right) exp(jax^2)\}_{k_x = 2ax, k_y = 0},
\end{aligned}
\tag{15}
$$

At the point, we are making an assumption that the constant a, is small enough so that $e^{jax^2} \approx 1$, then equation (15) becomes:

$$
t_1(x) = exp(jax^2) F\{P_1^*\left(\frac{k_0 x}{f}, \frac{k_0 y}{f}\right) P_2\left(\frac{k_0 x}{f}, \frac{k_0 y}{f}\right)\}_{k_x = 2ax, k_y = 0}. \tag{16}
$$

This assumption corresponds to the far field approximation in diffraction in that Fresnel diffraction becomes Fraunhofer diffraction [30]. Now we can express equation (16), besides some constant, in terms of the correlation integral:

$$t_1(x) = \exp(jax^2)[p_1(-\frac{fk_x}{k_0}, -\frac{fk_y}{k_0}) \otimes p_2(-\frac{fk_x}{k_0}, -\frac{fk_y}{k_0})]_{k_x=2ax, k_y=0}, \tag{17}$$

Similarly, equation (14) can be written as:

$$t_2(x) = \exp(-jax^2)[p_1(\frac{fk_x}{k_0}, \frac{fk_y}{k_0}) \otimes p_2(\frac{fk_x}{k_0}, \frac{fk_y}{k_0})]_{k_x=2ax, k_y=0}. \tag{18}$$

By putting equation (17) and equation (18) into equation (11), we have:

$$i_\Omega(x,y) = Re[i_{\Omega p}(x,y)\exp(j\Omega t),$$

Where

$$\begin{aligned} i_{\Omega p}(x) = I_0 &+ \frac{1}{2}\exp(jax^2)[p_1(-\frac{fk_x}{k_0}, -\frac{fk_y}{k_0}) \otimes p_2(-\frac{fk_x}{k_0}, -\frac{fk_y}{k_0})]_{k_x=2ax, k_y=0} \\ &+ \frac{1}{2}\exp(-jax^2)[p_1(\frac{fk_x}{k_0}, \frac{fk_y}{k_0}) \otimes p_2(\frac{fk_x}{k_0}, \frac{fk_y}{k_0})]_{k_x=2ax, k_y=0}, \end{aligned} \tag{19}$$

As we can see from equation (19), if we have a target object represented by p_1, and a reference object represented by p_2, we will, therefore, achieve the correlation of the two objects.

2.4 Real-time Pattern Recognition Without Using SLM In the Focal Plane

So far, we have given a brief overview of conventional real-time JTC systems with SLM in the focal plane. We also have introduced our hybrid optical system using optical heterodyne scanning. The purpose of this thesis is to realize real-time pattern recognition employing our new technique without using SLM in the focal plane. In this section, we will develop the optical system in the context of joint-transform correlation and describe an extraction scheme to display the correlation information without using any 2-D SLM in the focal plane to detect the power spectrum for real-time display.

Suppose we have two patterns $g_1(x, y)$ and $g_2(x, y)$ to be matched. The patterns are placed side by side in the front focal plane of lens L as shown in Figure.2. We let $p_1(x, y)=g_1(x-x_0, y)$ and $p_2(x, y)=g_2(x+x_0, y)$, and the Fourier Transform of these two patterns in the back focal plane forms a composite beam which is used to 1-D scan out a chirped grating which is given by $|T_0|^2 = 1+cos(ax^2)$. With the heterodyne current shown in equation (8) and the pattern information given by $p_1(x, y)$ and $p_2(x, y)$, we will have the heterodyne current out of the photo-detector as:

$$i_{\Omega p}(x) = I_0 + \frac{1}{2}exp(jax^2)A_{12}(\frac{-2axf}{k_0} - 2x_0, 0) + \frac{1}{2}exp(-jax^2)A_{12}(\frac{2axf}{k_0} - 2x_0, 0), \tag{20}$$

and equation (19) becomes:

$$\begin{aligned} i_{\Omega}(x) &= |I_0| cos(\Omega t + \theta_0) + \frac{1}{2}\left|A_{12}(\frac{-2axf}{k_0} - 2x_0, 0)\right| cos(\Omega t + ax^2 + \theta_1) \\ &+ \frac{1}{2}\left|A_{12}(\frac{2axf}{k_0} - 2x_0, 0)\right| cos(\Omega t - ax^2 + \theta_2), \end{aligned} \tag{21}$$

where θ_0, θ_1 and θ_2 are the phase angles of I_0, $A_{12}(\frac{-2axf}{k_0} - 2x_0, 0)$, and $A_{12}(\frac{2axf}{k_0} - 2x_0, 0)$, respectively. It should be noted that $i_{\Omega}(x)$ is a 1-D time signal as x is a function of time, i.e., $x(t)$, and this signal is an amplitude modulated signal with carrier Ω. The amplitude of the signal contains the correlation information, which can be extracted using a lock-in amplifier with reference signal equal to $cos(\Omega t)$. After the lock-in amplifier, from equation (21), we will have:

$$i_{lock-in}(x) \propto |I_0| cos(\theta_0) + \frac{1}{2}\left|A_{12}(\frac{-2axf}{k_0} - 2x_0, 0)\right| cos(ax^2 + \theta_1) + \frac{1}{2}\left|A_{21}(\frac{2axf}{k_0} - 2x_0, 0)\right| cos(ax^2 - \theta_2), \quad (22)$$

This can be displayed with a real-time monitor such as an oscilloscope. If $x(t)=vt$, that is the scanning position is linearly with time, where v is the constant scanning speed of the laser beam, equation (22) then manifests itself as two cross-correlations centered at two locations along the time scale: $t = \pm\frac{x_0 k_0}{vaf}$, and of course, the correlations are amplitude –modulated by the chirp-type functions $cos[a(vt)^2 + \theta_1]$ and $cos[a(vt)^2 - \theta_2]$.

From the definition of correlation as shown in equation (4), we can see, that the output heterodyne signal is the correlation between p_1 and p_2 carried on the transparency function. When the two patterns are identical and overlapped, the cross-correlation becomes autocorrelation, and low pass filtering will be expected. If the two patterns are identical but offset by a distance, band pass filtering will be achieved. Obviously, when the two patterns are perfectly matched, a strong correlation peak will be observed. Otherwise, the lower peak or a more flat line will be displayed.

In this case, if the two patterns $g_1(x, y)$ and $g_2(x, y)$ are placed side by side and perfectly matched, there will be two strong correlation peaks and since the y coordinates are zero within the correlation arguments, what we will really see is a line trace through the correlation peaks as y=0.

Until now, the theory for our real-time pattern recognition has been developed and discussed. According to the theory, we are able to set up the system to perform pattern recognition. The practical optical system used to demonstrate the principles discussed above will be presented in section 2.5, and the experimental result will be given in section 2.6.

2.5 Optical Implementation for Pattern Recognition

In this section, the experimental set up for optical pattern recognition is designed to demonstrate the principle that we gave in the previous section. Under the consideration of system's cost, reliability, complexity, and suitable for pattern recognition, the following system has been designed and the system diagram is shown in figure.3. We will explain the important component in this system and we will also show how the system works and several things that deserve careful attention.

Figure.3 shows the practical optical implementation of Figure.2 for real-time pattern recognition.

A good start to give an overview of this optical heterodyne scanning system is the optical source. Due to the low cost, high reliability, power safety and easy operation, a He-Ne laser has been employed in the experimental set up. The He-Ne laser is manufactured by Newport (λ=632.8*nm*), the power output from the He-Ne laser is about 15*mw*, which is strong enough for our purpose. In this implementation a Mach-Zehnder configuration is used to combine the two pupils. In order to get a heterodyne signal, the He-Ne laser directs the light into an acousto-optic modulator (AOM), which is driven by a 40MHz RF driver, operating at the Bragg regime at sound frequency $\Omega/2\pi \sim 40$MHz. The two diffracted beams, i.e., the zeroth-order beam and the first-order beam, are at frequencies ω_0 and $\omega_0+\Omega$. The AOM produces a fixed sound temporal-frequency $\Omega/2\pi \sim$ 40MHz offset between the two optical fields, which in turn are expanded by a 75x beam-expander. Lens L_1 served as a collimator to deliver two parallel beams: zeroth-order and first-order beams. After lens L_1, the zeroth-order beam is incident on the pattern p_1, and the first-order beam is incident on the other pattern p_2. The two patterns p_1 and p_2 are located at the front focal plane of lens L_2 with a focal length about 50cm. The two laser beams are combined together by Mirror M_1 and beam-splitter BS and then pass through lens L_2 which will form the Fourier transforms of P_1 and P_2 of patterns p_1 and p_2 in its back focal plane, respectively, projected through the galvanometer x-y scanner. In our case, for one-dimensional (1-D) scanning (which is the case used in our system), this structure can be simplified by using one of the galvanometer scan mirrors that we have already explained in the last section. Here we employed 1-D scan along the x-direction.

The scanning mirror can be controlled either by the computer or by the function generator. In our experiment, to obtain the stable scanning procedure, we used function generator to control the x-scanner. After the scanner, the two beams are focused onto the chirped grating located at the back focal plane of lens L_2. The chirp grating we used in our experiment is shown in figure 4. Lens L3 is used to collect all the light onto the photodetector (PD). The output signal from PD is sent to the signal input port of a SRS 488 RF lock-in amplifier. The purpose of using a lock-in amplifier is to achieve a better signal to noise ratio. The lock-in amplifier can amplify the signal even if the signal is within microvolts. The reference input of the lock-in amplifier comes from the same 40MHz RF driver, which is used to drive the AOM. By adjusting the sensitivity and time-constant of the lock-in amplifier, the current which given by equation (23) can be obtained through the lock-in amplifier. A 100MHz digital oscilloscope is used to display the correlation result in real time. The synchronized signal to the digital oscilloscope comes from the same function generator, which is used to drive the x scanner.

Due to this practical implementation, we are able to perform pattern recognition and obtain the recognition results. The experimental results are shown in section 2.6 and the discussion of the results is presented in section 2.7.

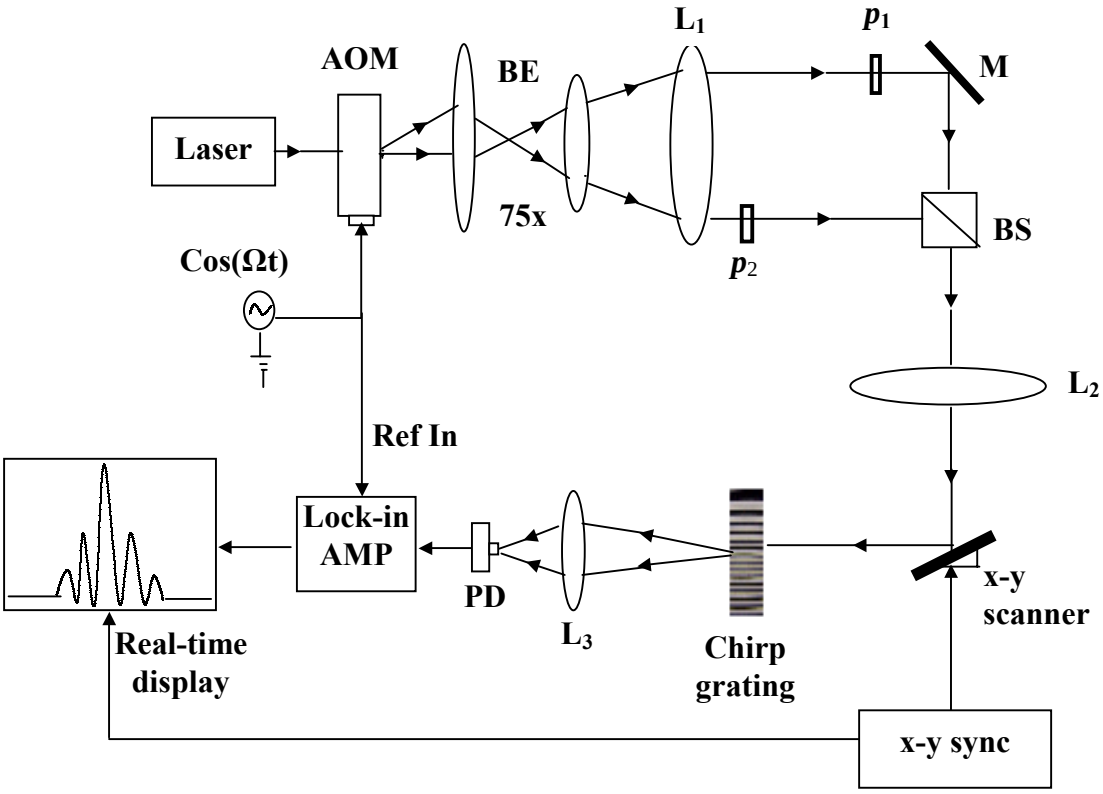

Figure.3 Practically used two-pupil optical pattern recognition heterodyning system

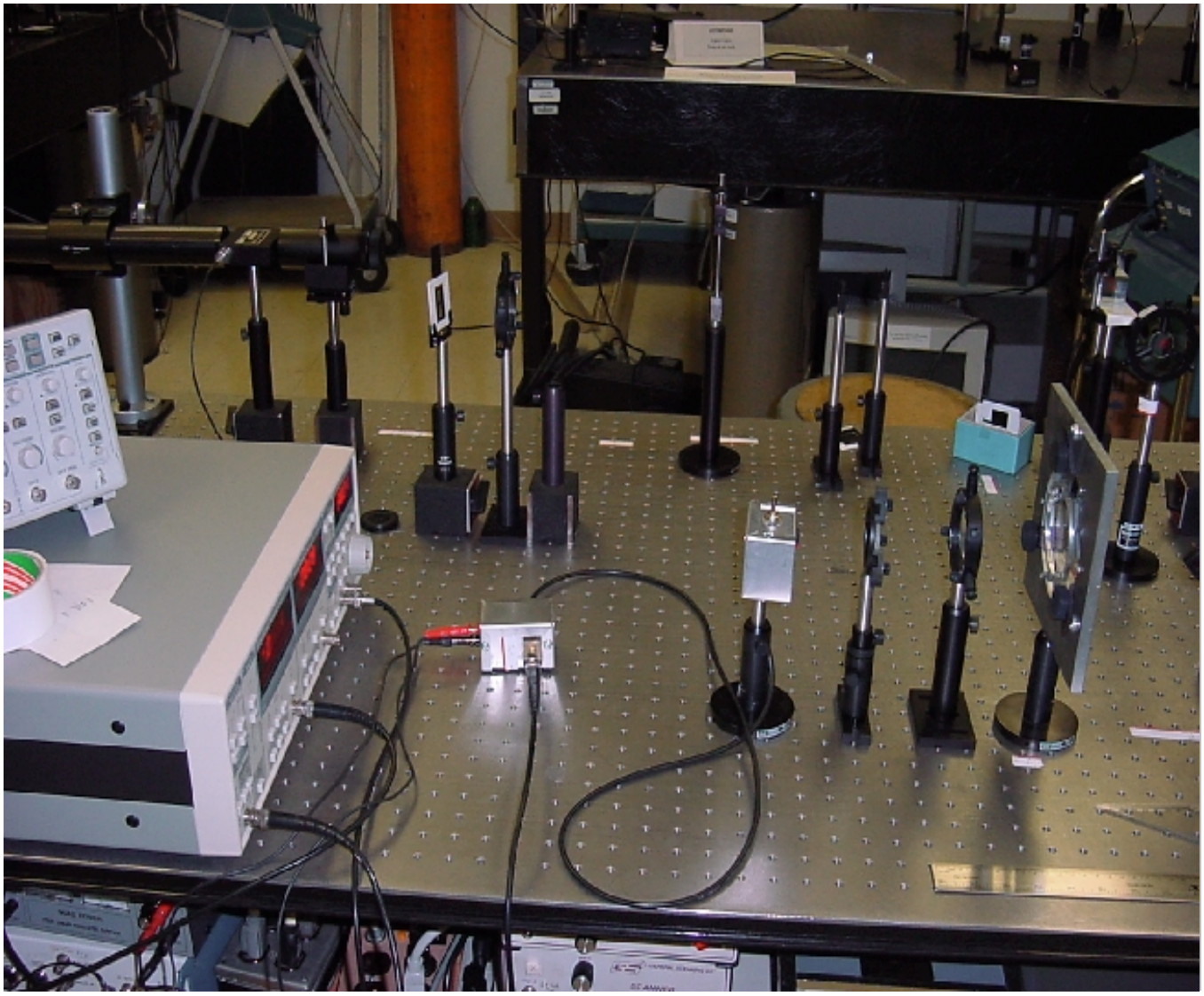

Figure. 3 (a) Implementation of real-time optical pattern recognition based on optical heterodyne scanning system

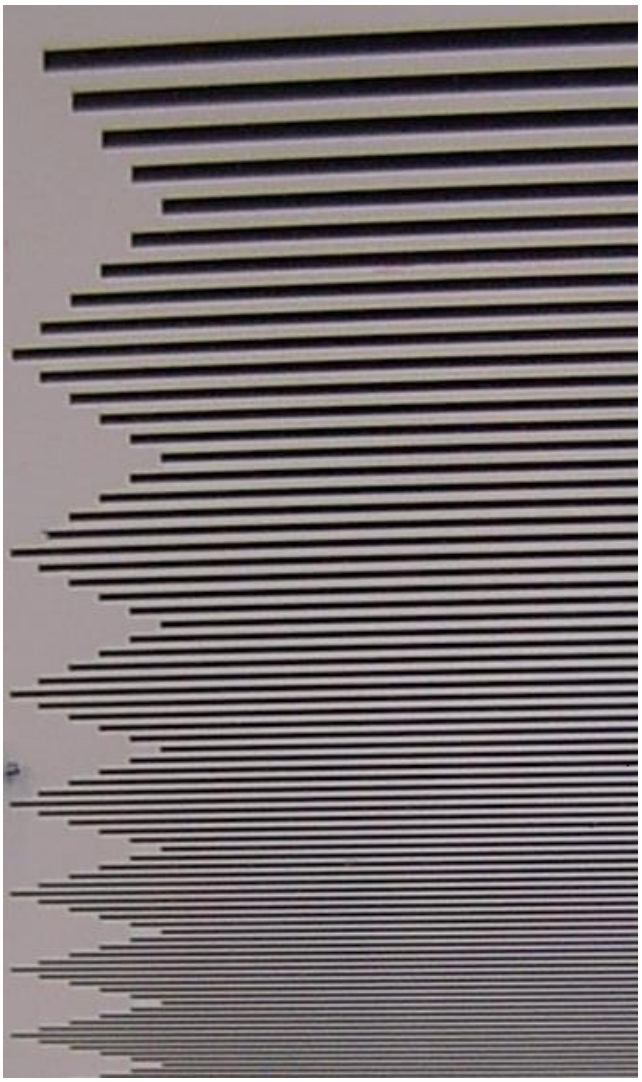

Figure. 4 1-D chirp grating

2.6 Experimental Results

The main goal of this experiment is to obtain the correlation result of two objects: one is the reference object, and the other is the target object. The result of this optical system is to effectively display the correlation result between the reference object and the target object. A strong correlation peak is expected if they are matched.

With the technique and the experimental set up discussed above, experiments using different reference objects and target objects have been performed. In order to compare the results between different experiments, all the system parameters, such as the power of laser source, the scan speed of X-Y scanner, the time constant and sensitivity of the lock-in amplifier, the voltage scale and time scale of the digital oscilloscope, are set to be the same values throughout these experiments.

In section 2.6.1, we will give some correlation results of two circular laser beams. Based on the performance shown in section 2.6.1, we then used different patterns as reference objects and target objects and obtained corresponding experimental results, which are shown in section 2.6.2.

2.6.1 Two Circular Apertures Correlation Results

Before we use complicated patterns as objects in our experiments, we have performed some preliminary experiments. We use two identical circular apertures as our two pupils. By adjusting the position of the mirror M or the beam-splitter BS as shown in figure 3, we can achieve two overlapped circular laser beams or two beams with a certain offset distance. As we have pointed out in the section 2.4, for two identical circular laser beams, we should expect a strong peak through the observation of a time trace signal in the digital oscilloscope. With the two identical beams overlapped, it will result in low-pass filtering of the object being scanned; with these two beams offsetting a certain distance, we expect band-pass filtering.

Based upon the above interpretations in filtering, the correlation results of using two identical circular apertures are shown in figure 5 and figure 6. In figure 5, the two circular beams are overlapped; we can see that at the low frequency range of the scanned chirped grating, the output signal is much stronger as compared with the high frequency range. The envelope of the waveform gives out a response characteristic of low-pass filtering. Similarly, in figure 6, since there is a distance offset between the two circular beams, the envelope of the waveform gives a response characteristic of band-pass filtering.

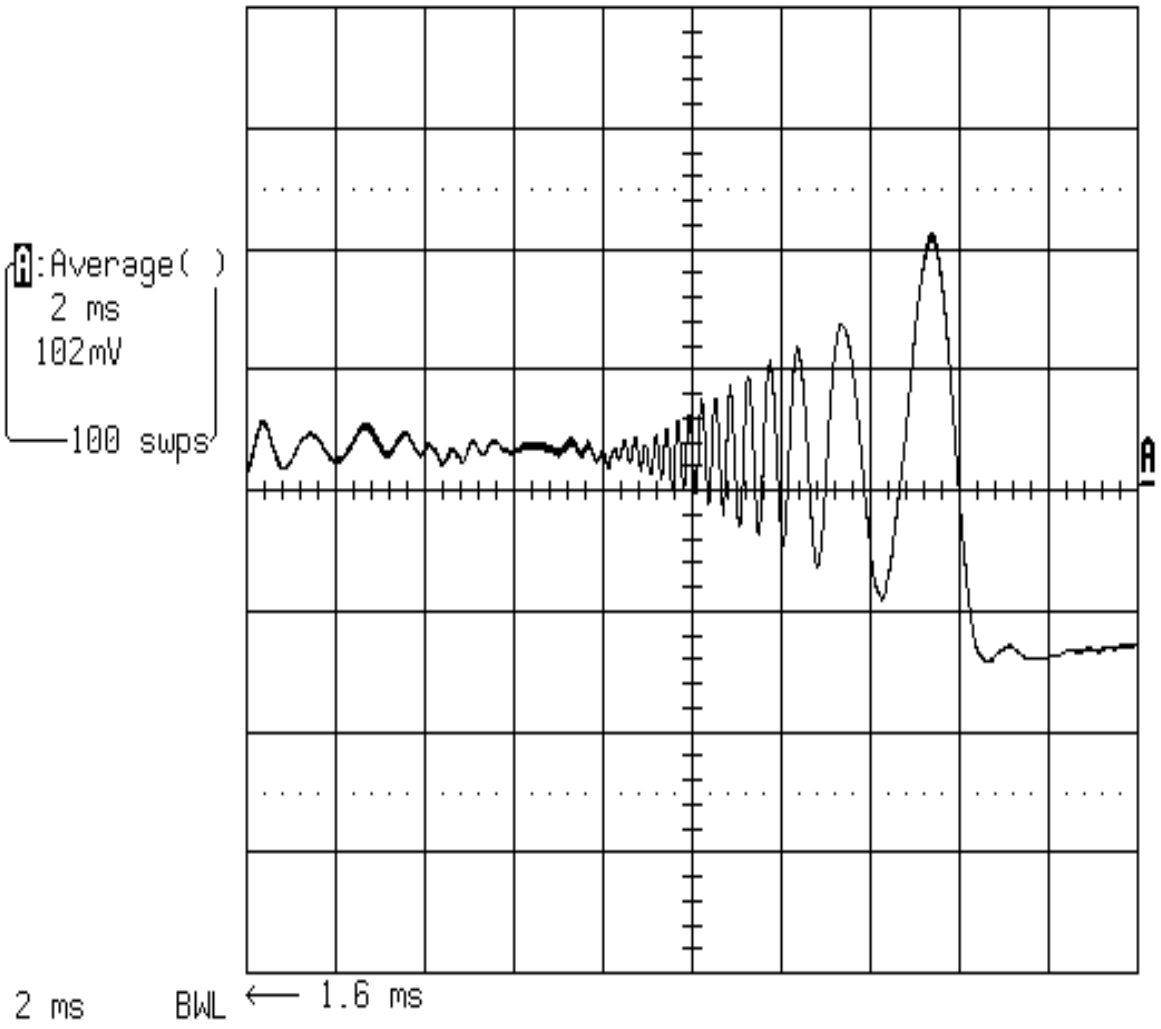

Figure. 5 Low-pass filtering resulted from two overlapped circular laser beams when scanning a 1-D chirped grating

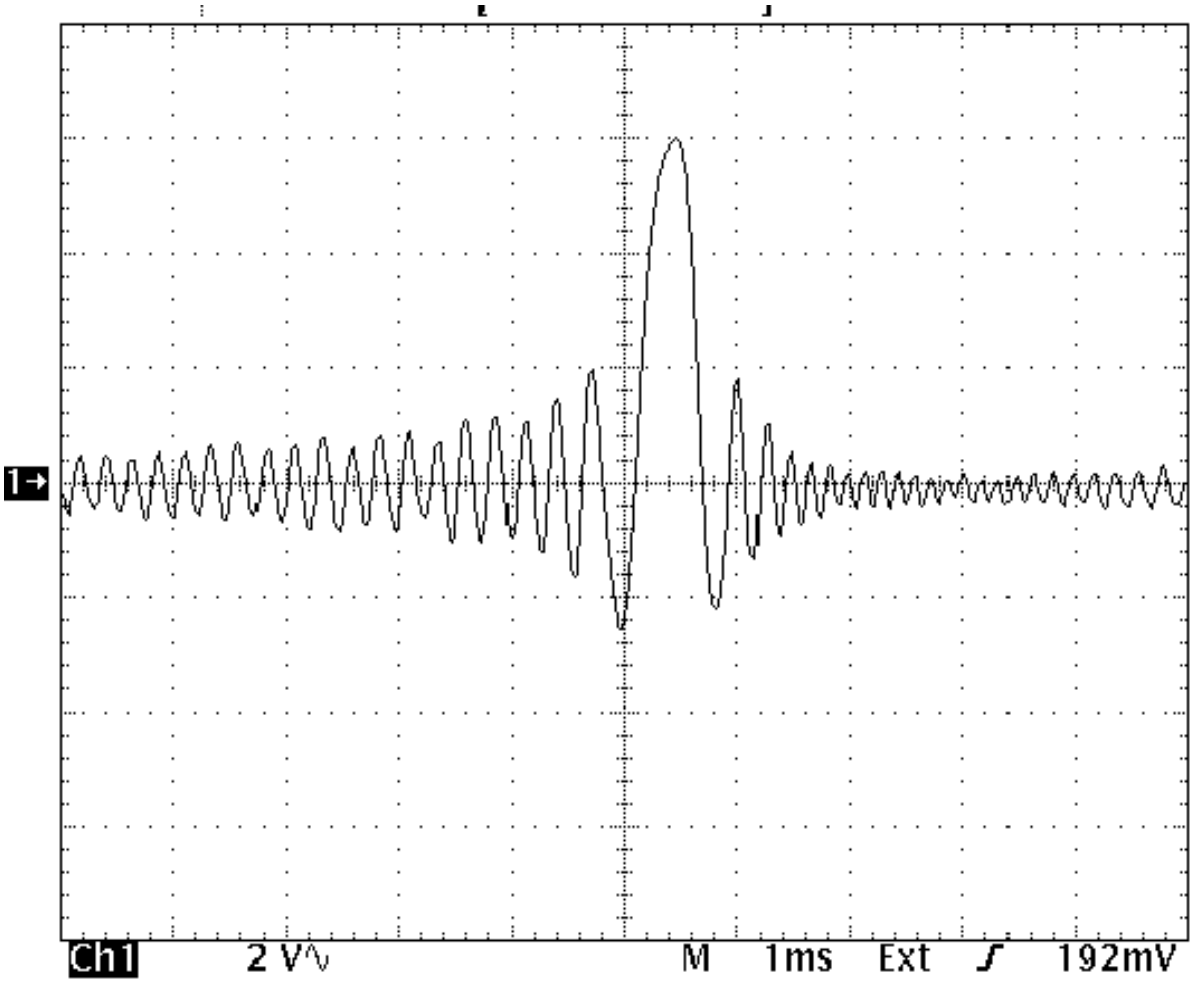

Figure. 6 Band-pass filtering resulted from two offset circular laser beams when scanning a 1-D chirped grating

2.6.2 Different Patterns Correlation Results

With the method and the results shown in section 2.6.1, experiments using different reference objects and target objects have been performed. In order to compare the results and see the difference between different experiments, we set all the system parameters, such as the power of the He-Ne laser source, the power and the frequency of the AOM driver, the separated distance between the two patterns that need to be matched, the scanning speed of the x-y scanner, the time constant and sensitivity of the lock-in amplifier, the voltage scale and the time scale of the digital oscilloscope, to the same values throughout our experiment.

We used two different reference objects: animal 1 and a random pattern given by figure 7. For the reference object goat, we used four different target objects, (four animals) given by figure 8 to do the correlation with animal 1. Compared with the random pattern, these patterns contain fewer details. For the random pattern we used two different patterns given by figure 9 to do the corresponding correlation.

Figure 10 through figure 13 show the correlation results of the four animals with reference pattern animal 1. Figure 14 and figure 15 show the correlation results of the target patterns shown in figure 9 with the reference random pattern. Discussion of the experimental results is presented in section 2.7.

Reference pattern 1: animal 1

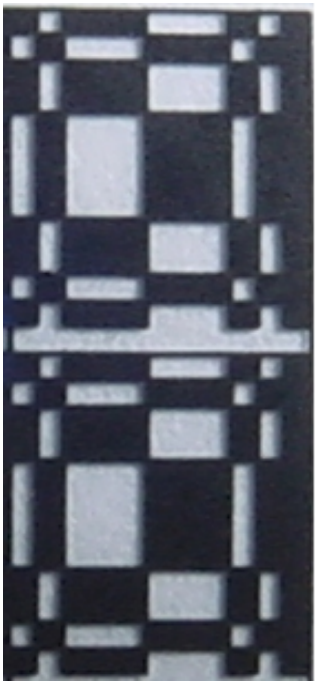

Reference pattern 2: random pattern

Figure. 7 Two different reference patterns

Animal 1

Animal 2

Animal 3

Animal 4

Figure. 8 Four target patterns: animal 1 to animal 4

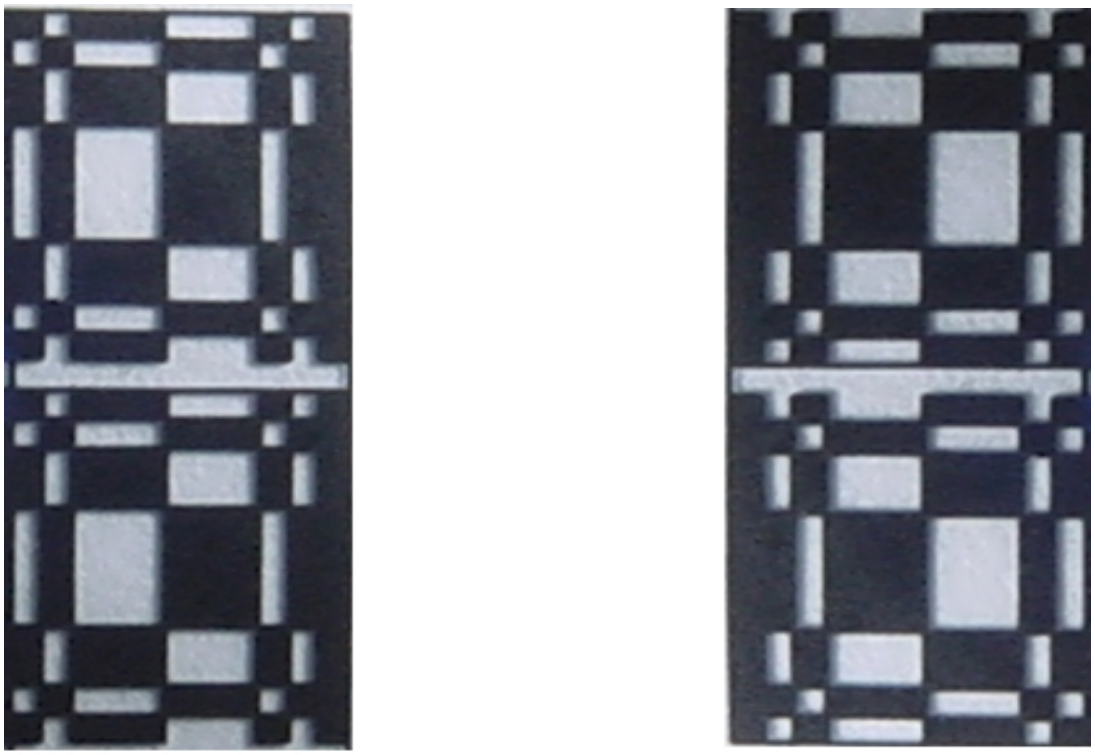

Random pattern **Reversed random pattern**

Figure. 9 Two target patterns

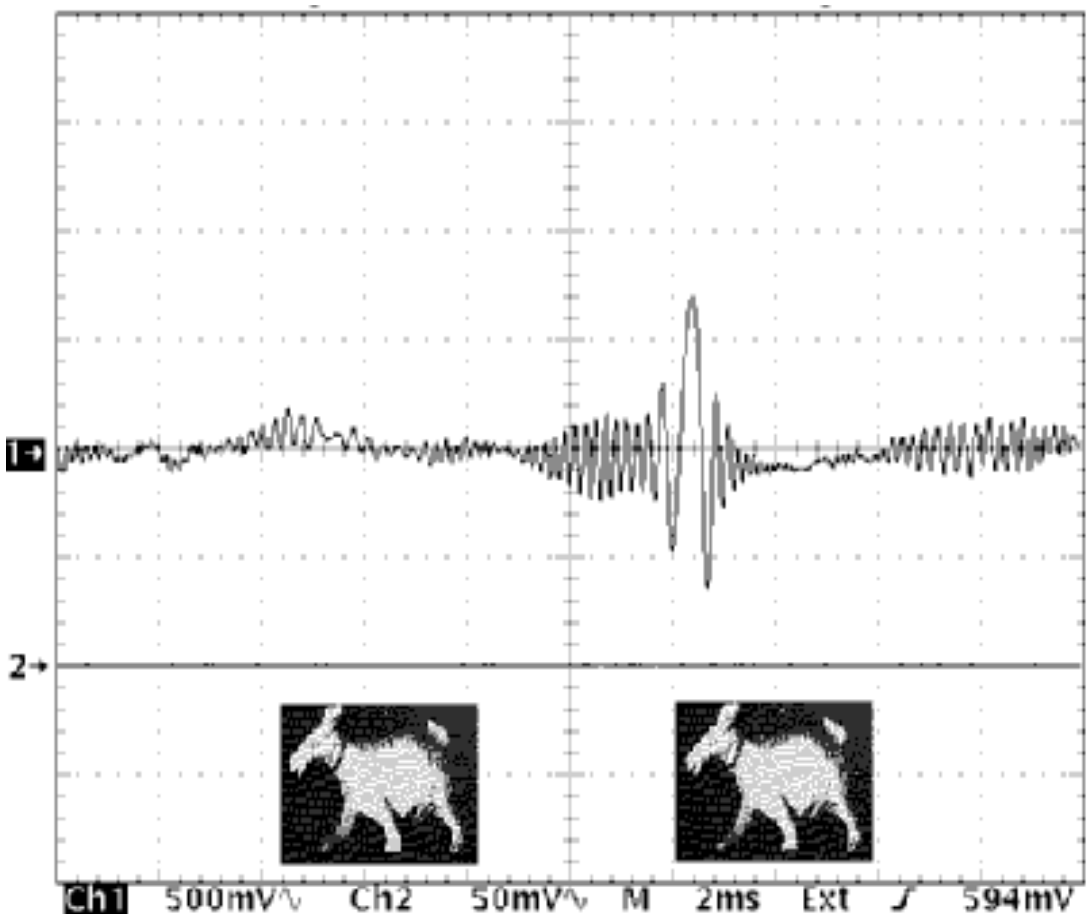

Figure. 10 autocorrelation of Animal 1 with Animal 1

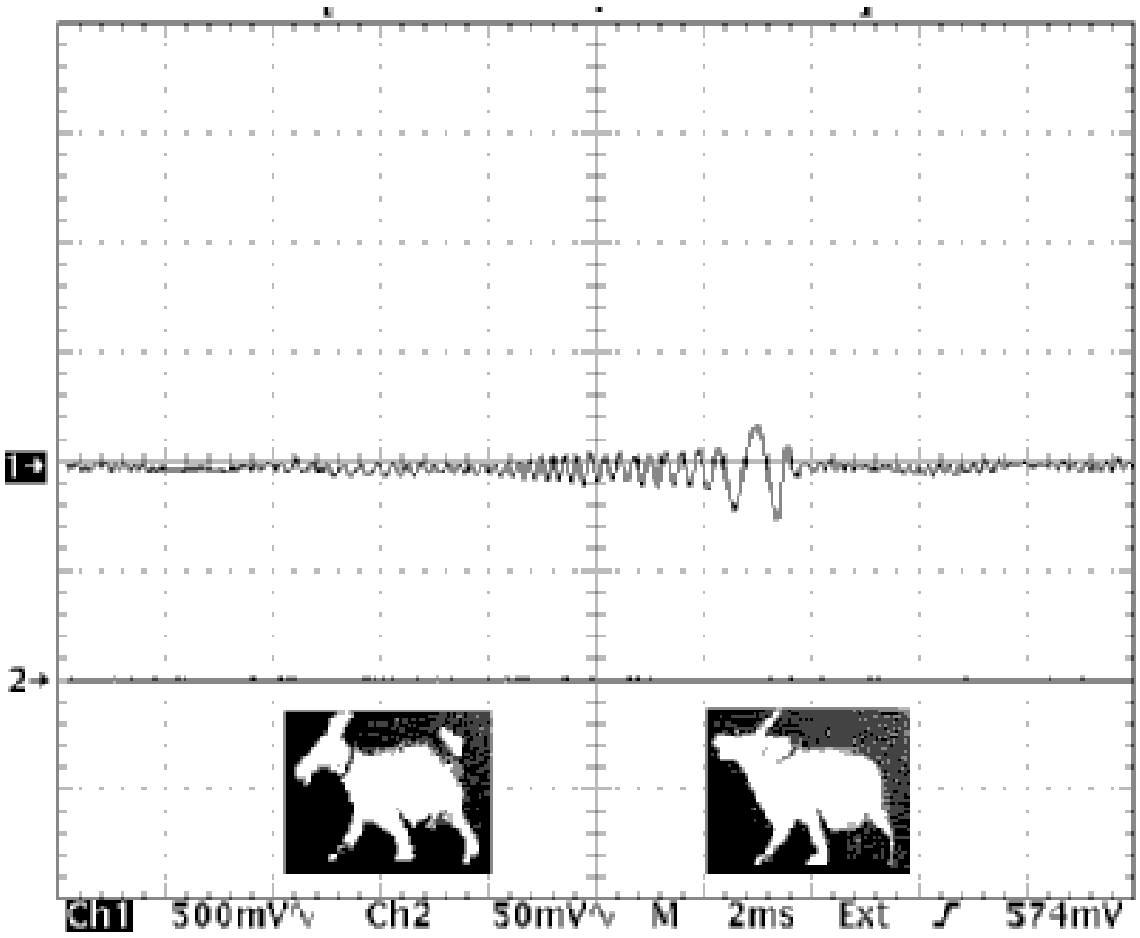

Figure. 11 cross-correlation of Animal 1 with Animal 2

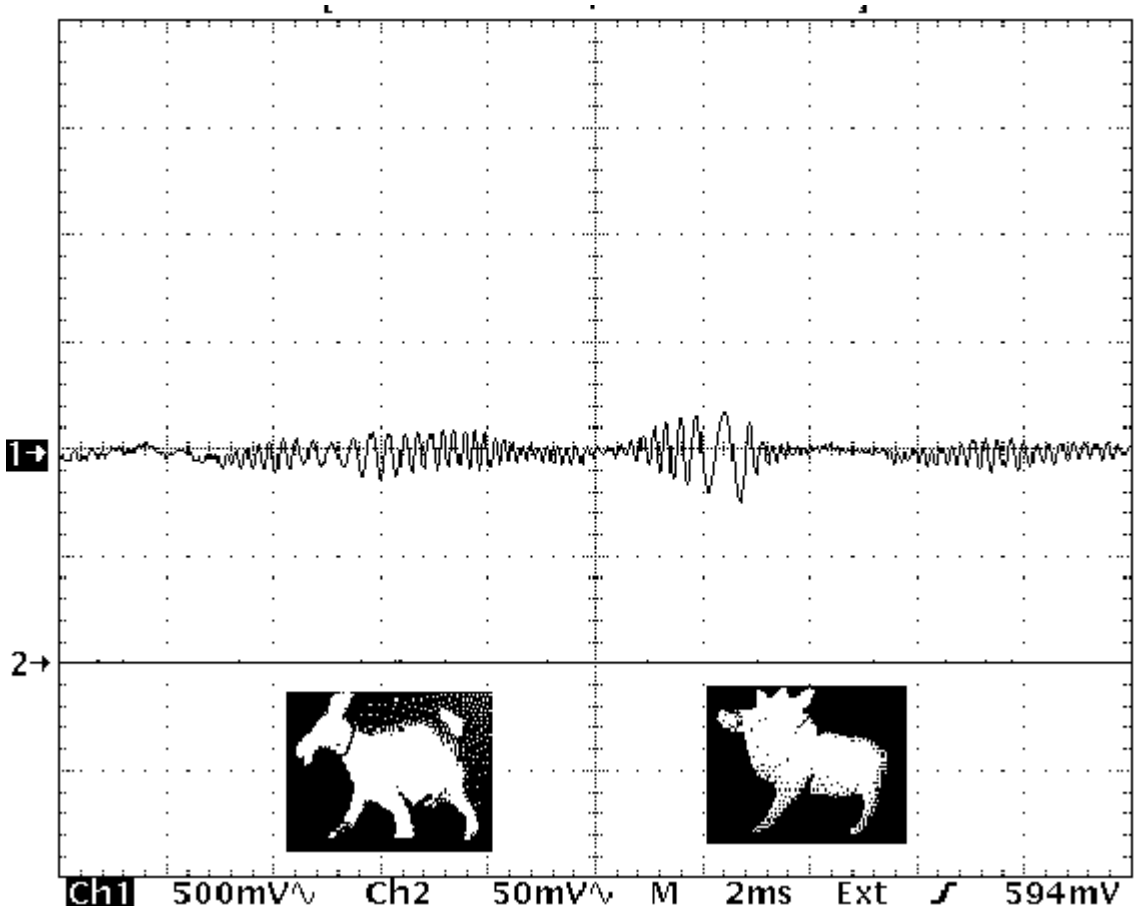

Figure. 12 cross-correlation of Animal 1 with Animal 3

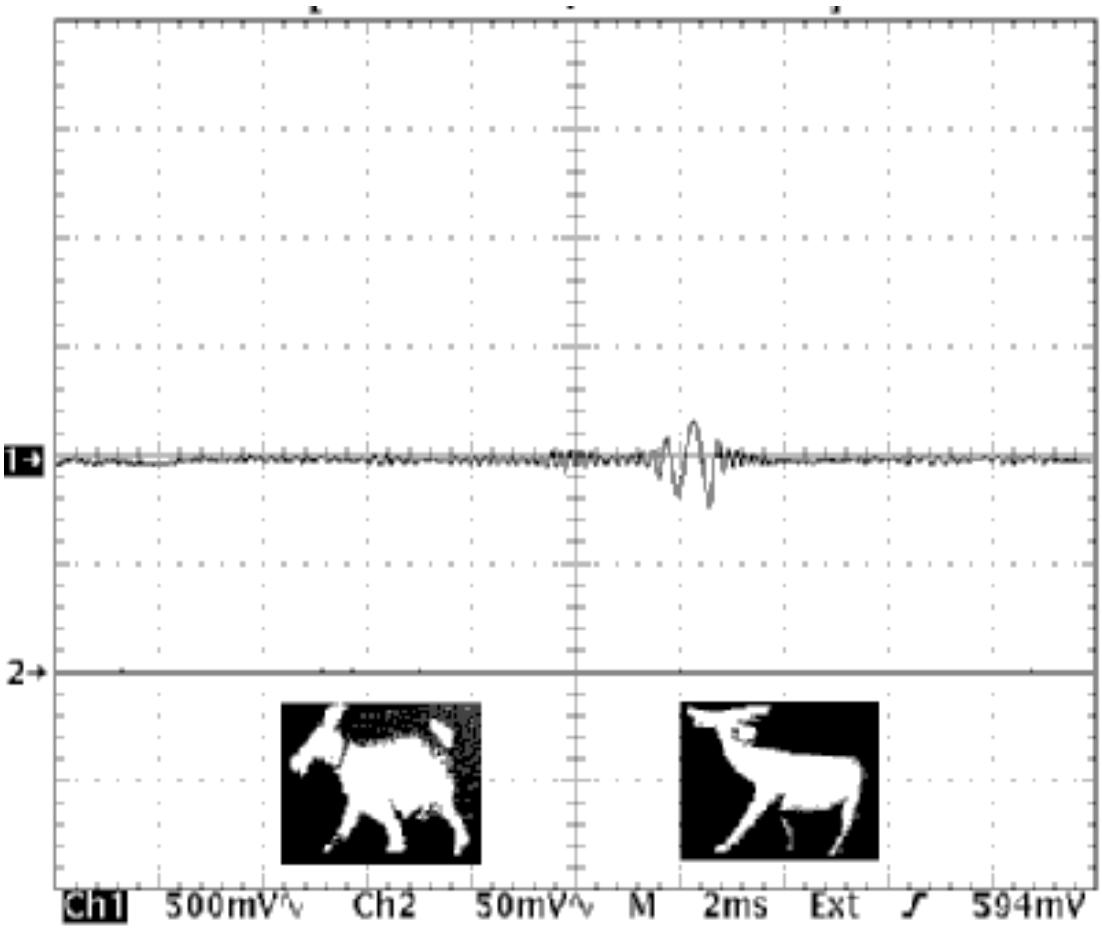

Figure. 13 cross-correlation of Animal 1 with Animal 4

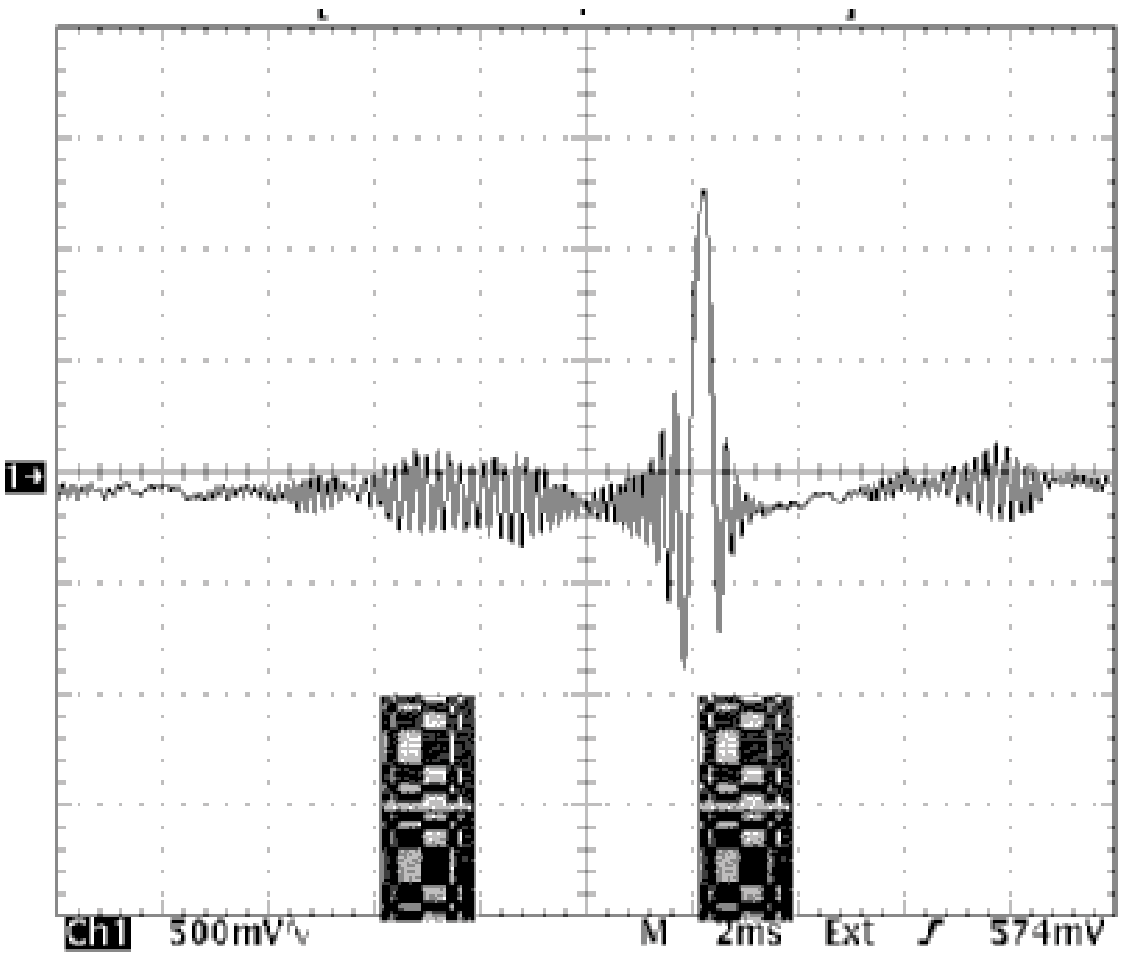

Figure. 14 autocorrelation of random pattern with random pattern

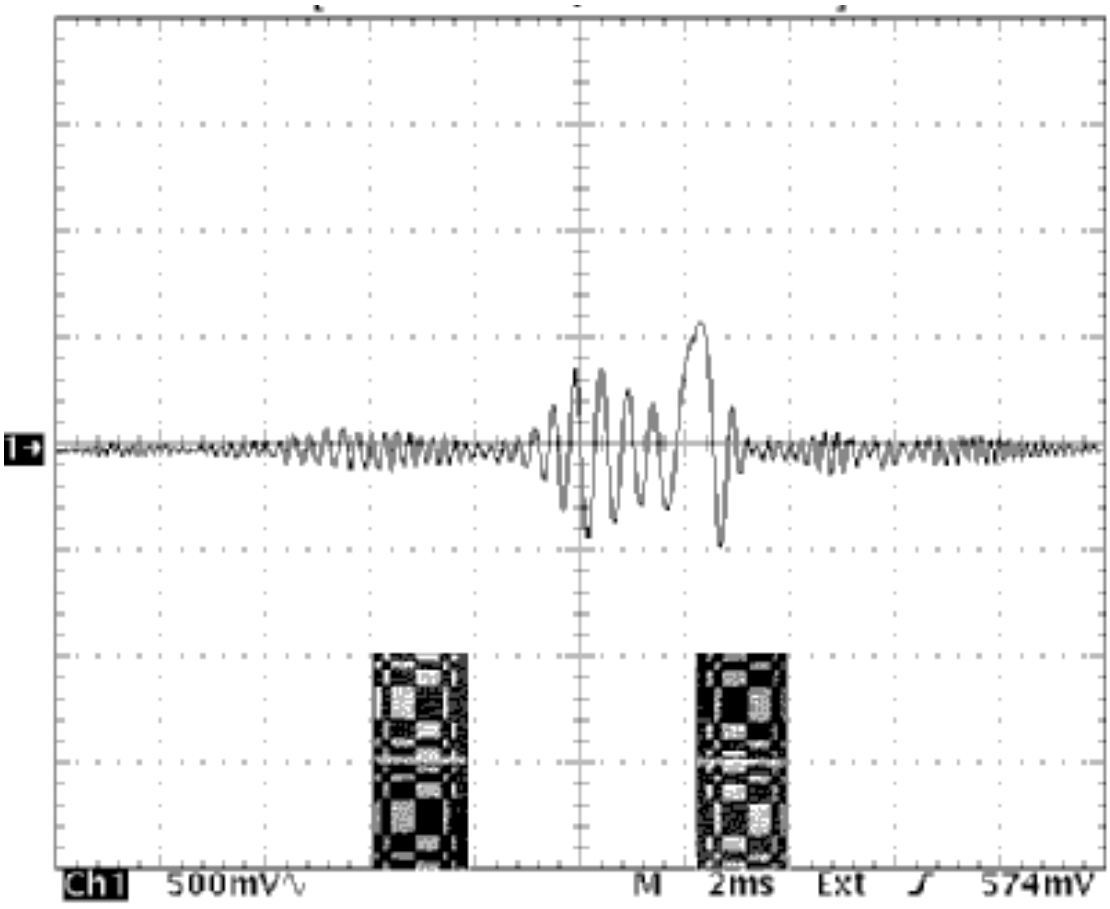

Figure. 15 cross-correlation of random with inversed random pattern

2.7 Discussion of Results

In the previous sections, we proposed the theory of our heterodyne scanning system, pointed out the advantage of our new JTC system, described the experimental set up and presented the experimental results as we expected. To qualify these claims, we will analyze the experimental results in detail, such as the size of the pattern, the distance between the reference and target objects, etc. With the concern of the content of the patterns, in this section, we will address the difference among these results regarding the less or more information provided by the patterns.

Figure 10 shows two identical patterns animal 1 and animal 1 with the size about $6mm \times 7mm$, shown on the bottom of the figure. They are placed at the front focal plane of lens L_2 of focal length of *50cm* for autocorrelation. The two patterns are separated by $2x_0 = 6mm$, which gives the center peak frequency $2x_0/\lambda f \sim 20$ *cycle/mm*. When a chirped grating is 1-D-scanned along the *x*-direction, a trace of electrical signal through the center of the autocorrelation will be displayed (see equation (22)). Indeed, we see a strong peak display on the oscilloscope as shown in the figure. The time scale is 2ms per division with vertical scale of *500mv* per division. Figure. 4 shows the picture of the chirped grating that we used in our experiment. It is basically a set of dark lines of varying separations, printed on a glass substrate. The grating frequency ranges from *1 cycle/mm* to *25 cycle/mm*. Since the grating used is not symmetrical, we only observed a single correlation peak.

In figure 11 through figure 13, the cross-correlation between target objects (animal 2, animal 3 and animal 4) and reference object (animal 1) are presented. The target objects are the same size as the reference object (animal 1). For convenient comparison, the distance between the reference pattern and the target pattern is the same as the distance we described in figure 10. If the two patterns are perfectly matched, the center peak frequency will be the same as shown in figure 10. As we can see from these figures, the autocorrelation peak in figure 10 is about 3 times higher than the cross-correlation peak shown in figure 11 to figure 13, which indicates that animal 1 is not well matched with the other three animals.

The random pattern we used in this experiment provides more structural details than the pattern of the four animals. Due to this aspect, we can expect the autocorrelation

peak to be stronger and sharper as it is evident from figure 14, where two identical random patterns with size of $3mm \times 8mm$ are used. The random patterns are apart by $2x_0 = 3mm$, which gives $2x_0/\lambda f \sim 10\ cycle/mm$. It clearly shows the result as we expected. Figure 15 shows the cross-correlation when the random patterns and its contrast reversed random pattern are used. The correlation peak is much lower than the one in figure 14 as expected and verified.

Several other patterns have been used in this experiment; the results turned out are exactly the kind that we expected. Due to some critical conditions, (such as, the optical alignment), the ability of how much light can pass through the pattern, (which will result the final intensity of the light collected by the photo detector) will be affected, with the final results displayed on the digital oscilloscope. However, with modern technology (precision instrument and better alignment), it is possible to improve the reliability of the system, and get high-resolution result.

So far, we have given some analysis about the experimental results and the fundamental difference among these results is interpreted. To support our theory, computer simulations have also been considered and performed to make our new JTC system more believable, and to make this work more successful.

Computer simulation results are presented in chapter 3.

Chapter 3. Computer Simulation Results

To effectively confirm the experimental results shown in section 2.6, MATLAB programs have been developed to do the simulations corresponding to the experimental results shown in section 2.6.

In this chapter, first, we will show the computer read out patterns, which are the same as we used in the experiment with resolution 64×64 pixels. We are then going to show the correlation results that have been done by the computer.

Figure 16 through figure 39 show the computer simulation results for the reference patterns with target patterns we used for our experiment. From these results, we may see the similarity between the experimental results and the computer simulation results. Computer simulation results are less noisy than the one we achieved through experiment.

The MATLAB program for the simulation is shown in Appendix A.

Computer Simulation Results:

1. Animal 1 with Animal 1:

A. Two patterns read out by computer:

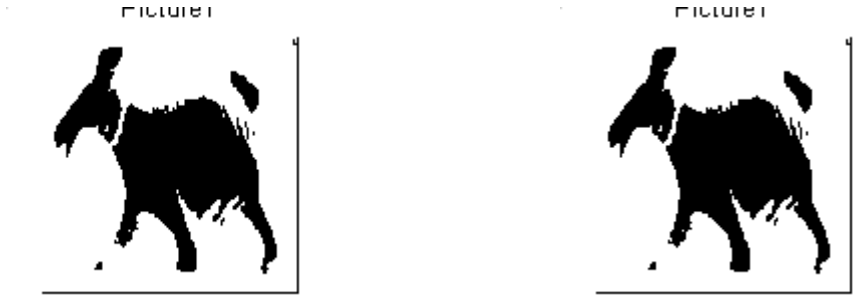

Figure. 16 Reference pattern animal 1 and target pattern animal 1 read out by computer

B. 3-D correlation result—reference pattern Animal 1 with target pattern Animal 1:

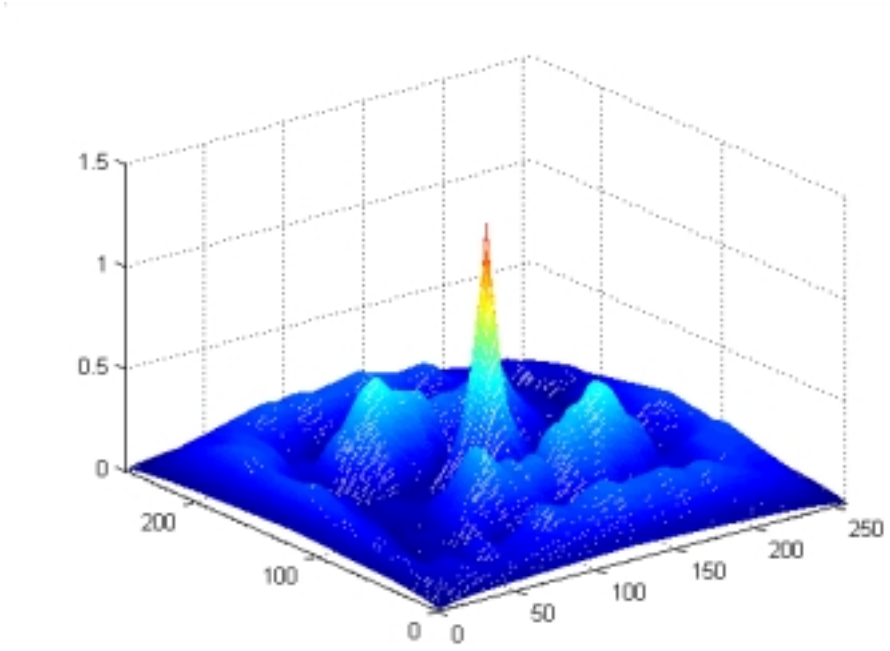

Figure. 17 3-D correlation results of Animal 1 with Animal 1

C. 1-D correlation results:

(1). Patterns Animal 1 and Animal 1 are overlapped:

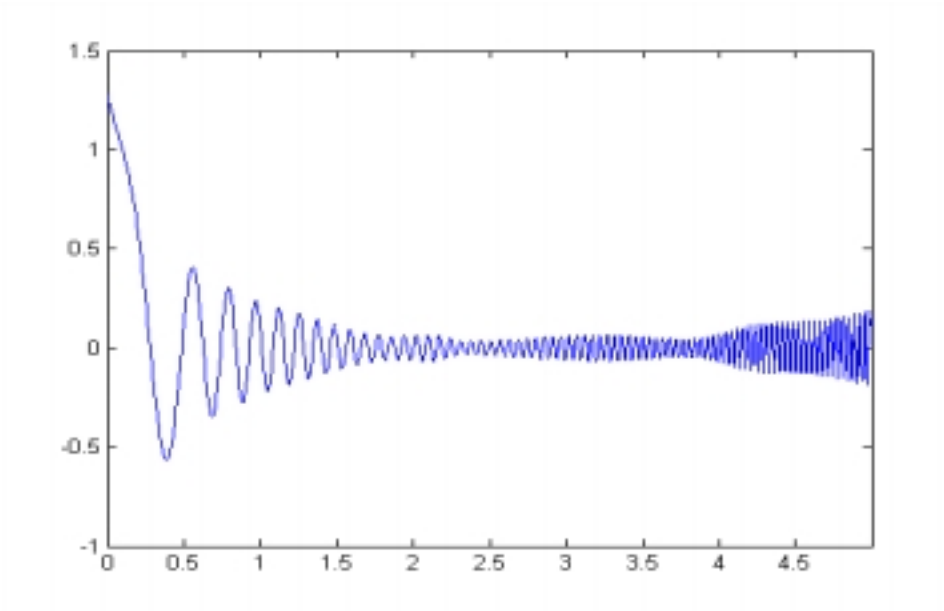

Figure. 18 1-D correlation result for Animal 1 with Animal 1 overlapped

(2) Patterns Animal 1 and Animal 1 are side by side:

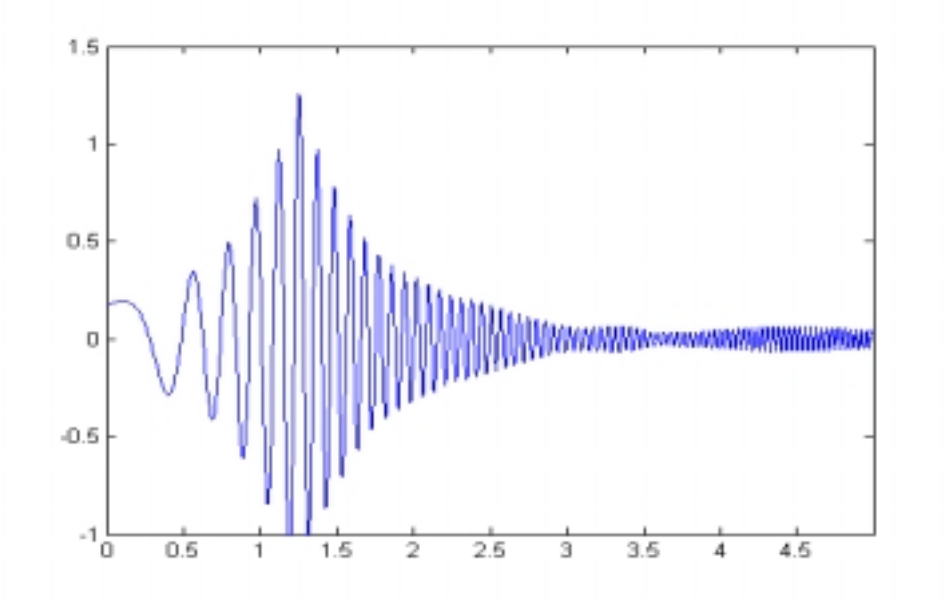

Figure. 19 1-D correlation result for Animal 1 with Animal 1 side by side

2. Animal 2 and Animal 1:

D. Two patterns read out by computer:

Figure. 20 Reference pattern animal 1 and target pattern animal 2 read out by computer

E. 3-D correlation result—reference pattern Animal 1 with target pattern Animal 2:

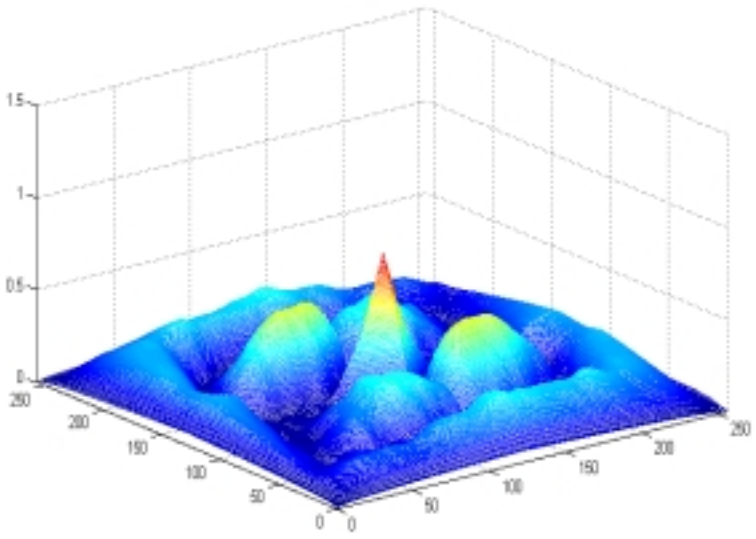

Figure. 21 3-D correlation results of Animal 1 with Animal 2

F. 1-D correlation results:

(1). Patterns Animal 1 and Animal 2 are overlapped:

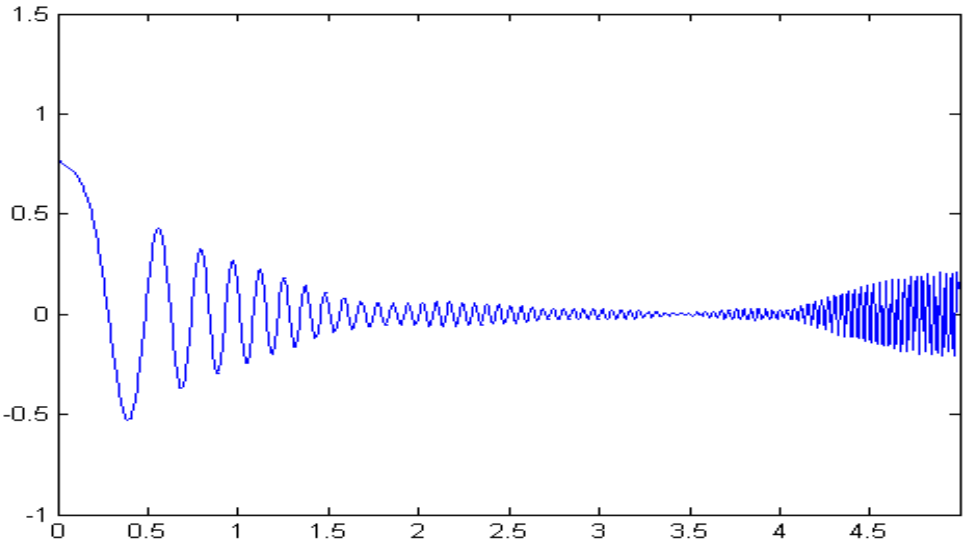

Figure. 22 1-D correlation result for Animal 1 with Animal 2 overlapped

(2) Patterns Animal 1 and Animal 2 are side by side:

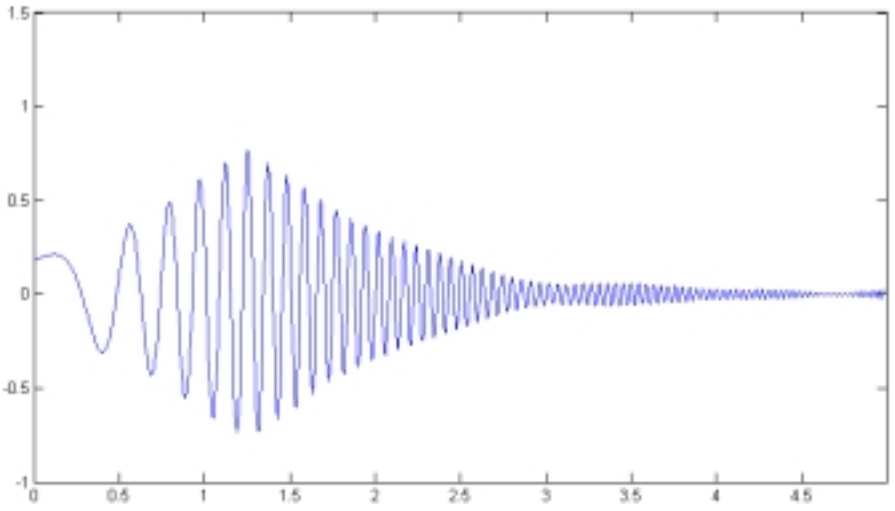

Figure. 23 1-D correlation result for Animal 1 with Animal 2 side by side

3. Animal 3 and Animal 1:

G. Two patterns read out by computer:

Figure. 24 Reference pattern animal 1 and target pattern animal 3 read out by computer

H. 3-D correlation result—reference pattern Animal 1 with target pattern Animal 3:

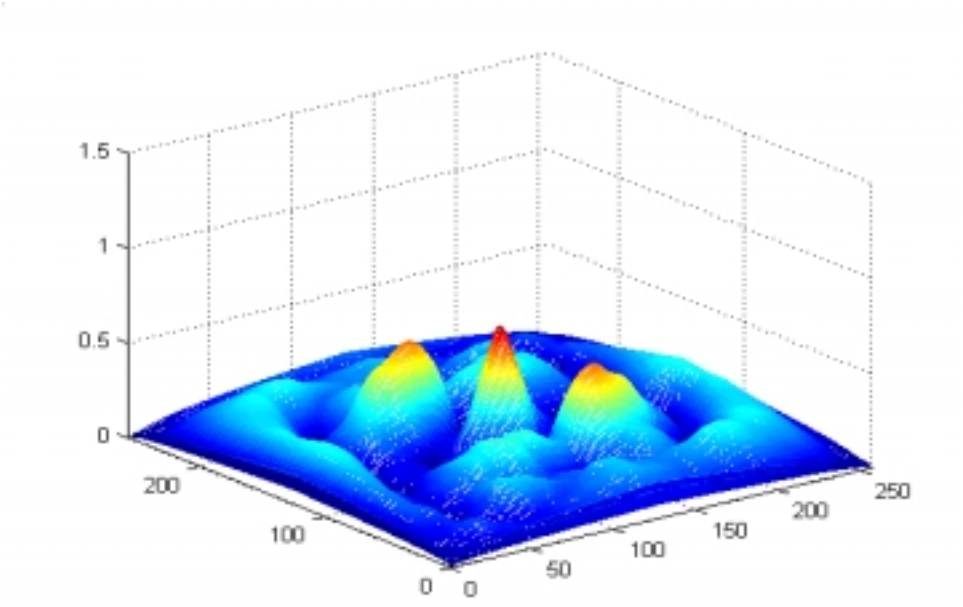

Figure. 25 3-D correlation results of Animal 1 with Animal 3

I. 1-D correlation results:

(1). Patterns animal 1 and animal 3 are overlapped:

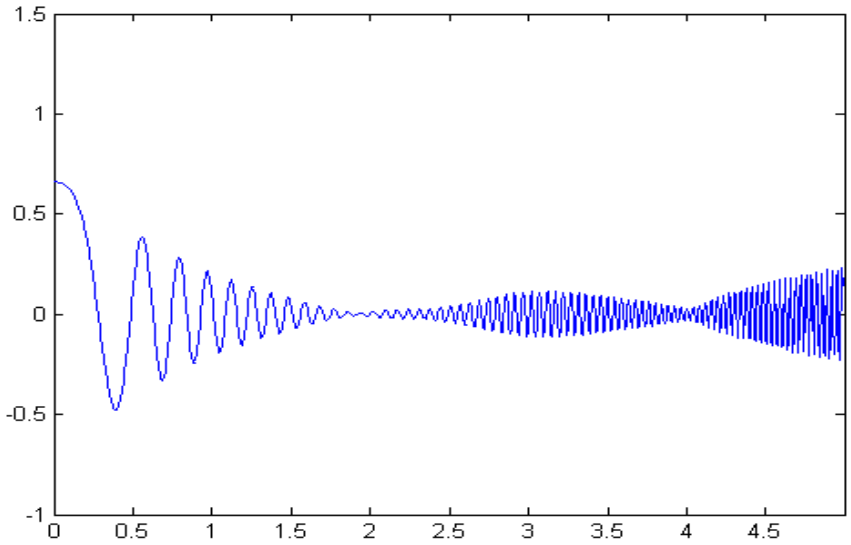

Figure. 26 1-D correlation results for Animal 1 with Animal 3 overlapped

(2) Patterns Animal 1 and Animal 3 are side by side:

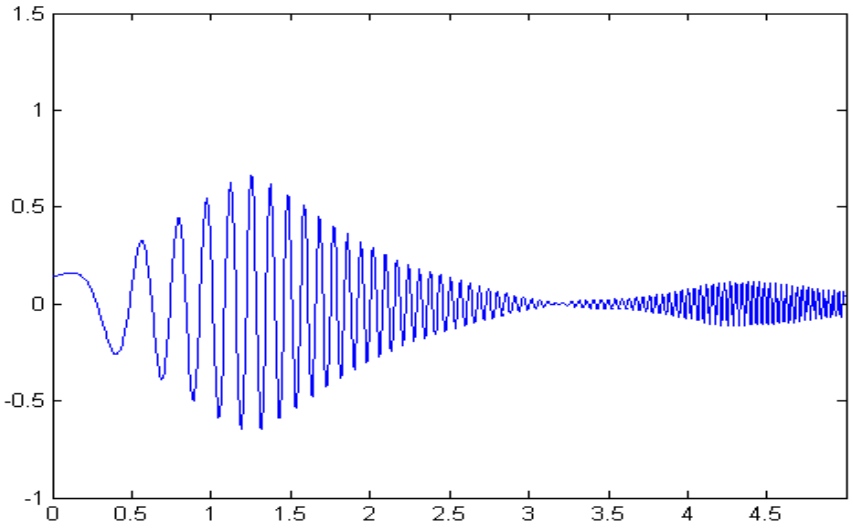

Figure. 27 1-D correlation result for Animal 1 with Animal 3 side by side

4. Animal 4 and Animal 1:

G. Two patterns read out by computer:

Figure. 28 Reference pattern Animal 1 and target pattern Animal 4 read out by computer

J. 3-D correlation result—reference pattern Animal 1 with target pattern Animal 3:

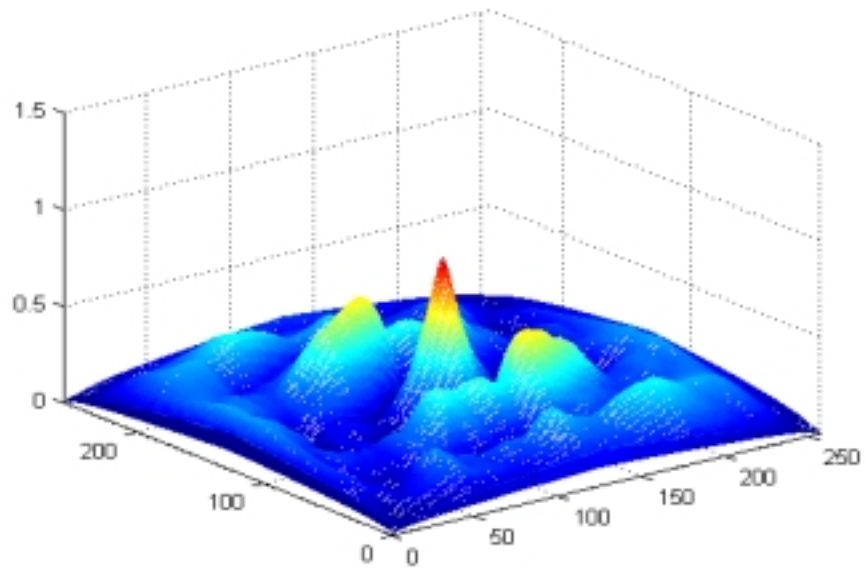

Figure. 29 3-D correlation results of Animal 1 with Animal 3

K. 1-D correlation results:

(1). Patterns Animal 1 and Animal 4 are overlapped:

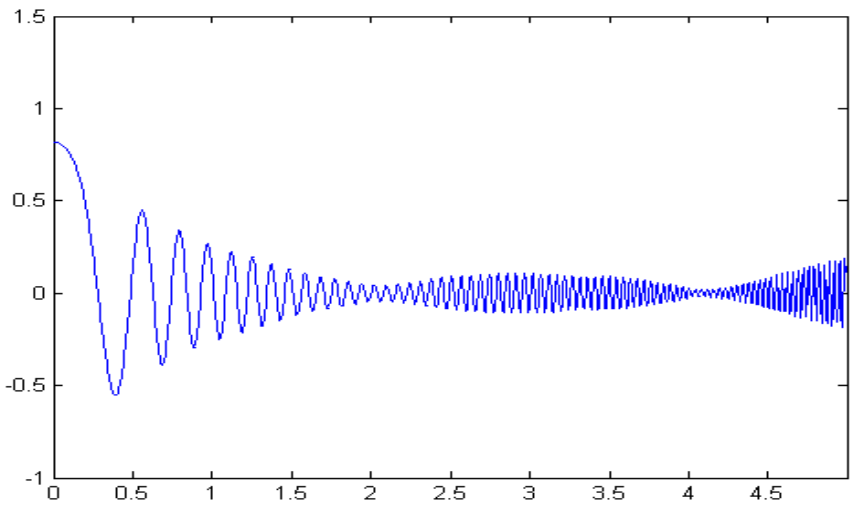

Figure. 30 1-D correlation results for Animal 1 with Animal 4 overlapped

(2) Patterns Animal 1 and Animal 4 are side by side:

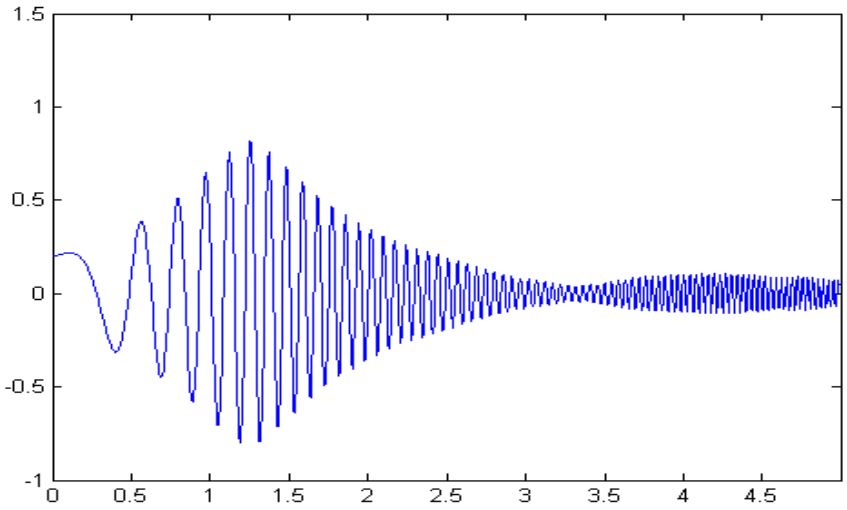

Figure. 31 1-D correlation result for Animal 1 with Animal 4 side by side

5. Random pattern and reversed random pattern:

L. Two patterns read out by computer:

Figure. 32 Reference random pattern and target random pattern read out by computer

M. 3-D correlation result—reference random pattern with target random pattern:

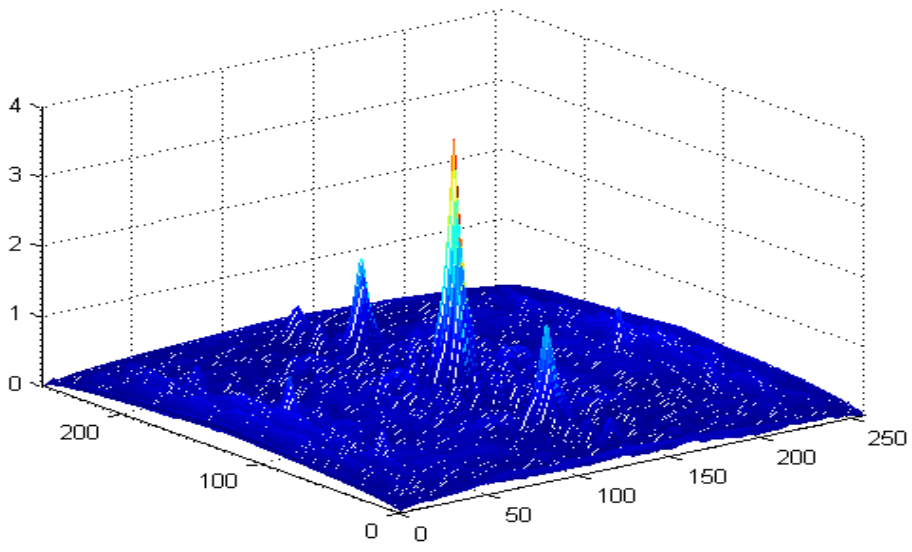

Figure. 33 3-D correlation results of random pattern with random pattern

N. 1-D correlation results:

(1). Random pattern and random pattern are overlapped:

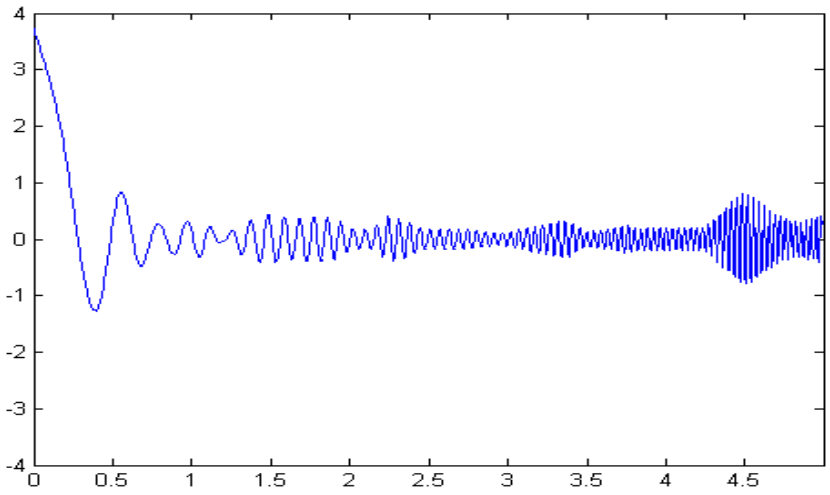

Figure. 34 1-D correlation result for random pattern with random pattern are overlapped

(2) Random pattern and random pattern are side by side:

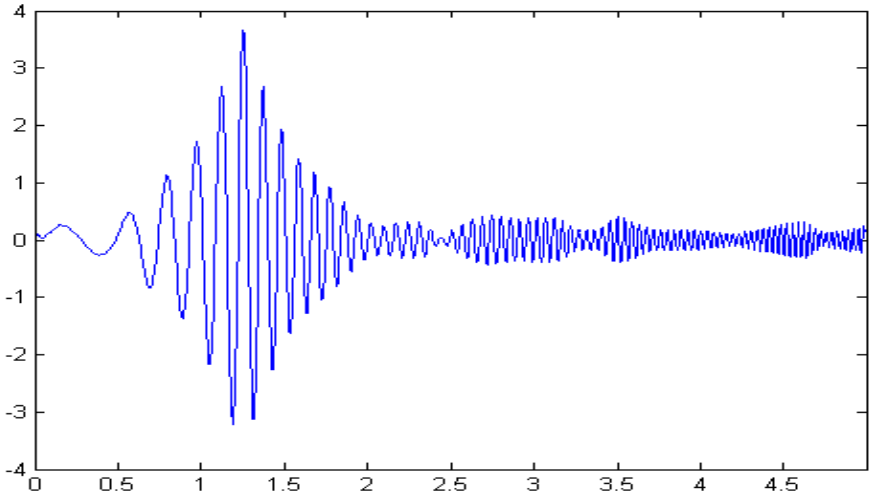

Figure. 35 1-D correlation result random pattern with random pattern side by side

6. Random pattern and reversed random pattern:

O. Two patterns read out by computer:

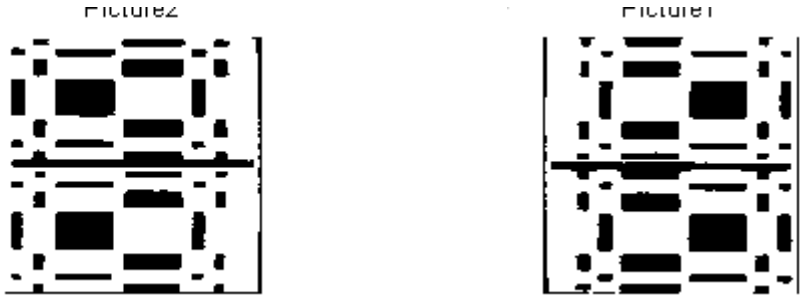

Figure. 36 Reference random pattern and target reversed random pattern read out by computer

P. 3-D correlation result—reference random pattern with target reversed random pattern:

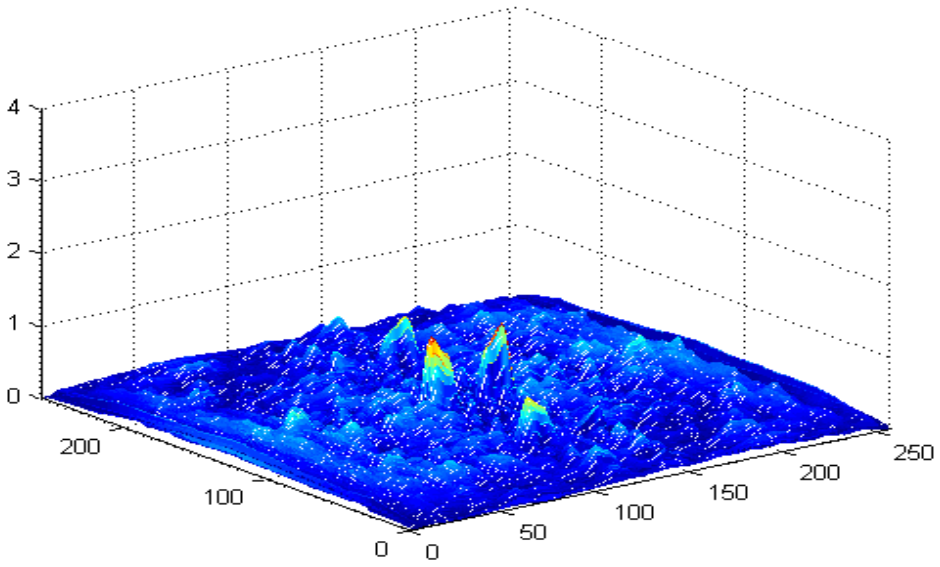

Figure. 37 3-D correlation results of random pattern with reversed random pattern

Q. 1-D correlation results:

(1). Random pattern and reversed random pattern are overlapped:

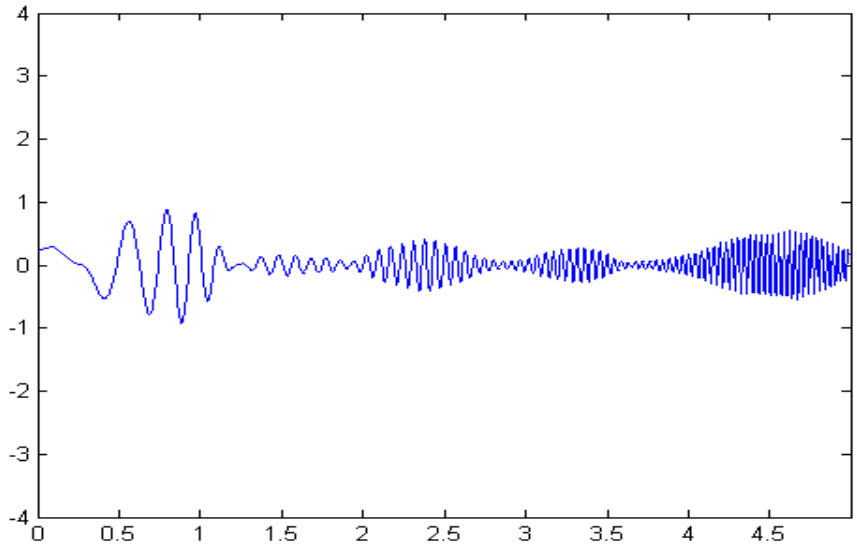

Figure. 38 1-D correlation results for random pattern with reversed random pattern are overlapped

(2) Random pattern and random pattern are side by side:

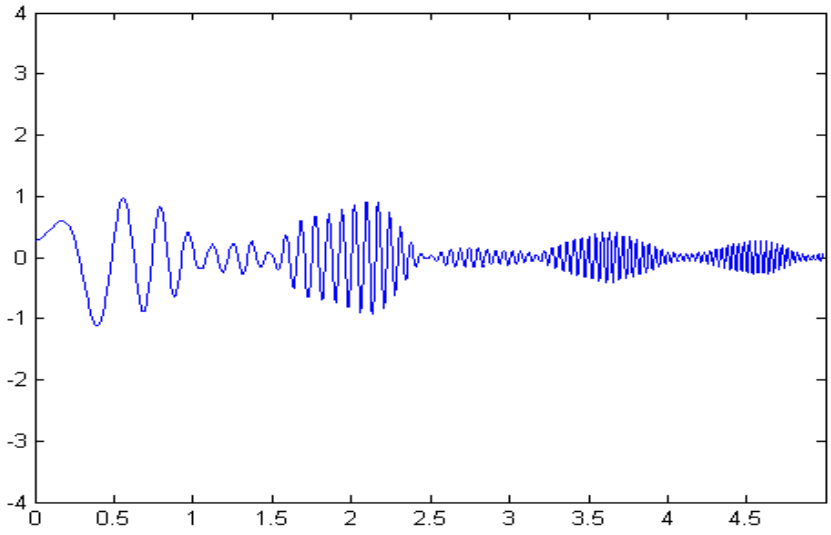

Figure. 39 1-D correlation result for random pattern with reversed random pattern side by side

Chapter 4. Conclusion

4.1 Summary of the Work

The objective of this thesis is to provide a novel real-time joint-transform correlator without the use of any 2-D spatial light modulator located at the Fourier plane. The important part of this thesis was concerned with real-time optical pattern recognition using our optical-electronic hybrid system, which is based on optical heterodyne scanning. In the end, pattern recognition results were obtained through the implementation of optical heterodyne scanning pattern recognition system.

The fundamental idea concerning optical pattern recognition has been was introduced in chapter 1. As one of the most important mathematical operations in image processing and pattern recognition, the correlation of two patterns has been studied over a decade. IN considering the traditional systems employing spatial light modulators (SLMs), the drawbacks of using SLMs have been pointed out and a new optical pattern recognition method has been proposed without these drawbacks.

In chapter 2, we first gave a brief overview of the standard architecture of a joint-Transform correlation system; the basic knowledge of the two-pupil heterodyning system was then presented. When a chirped grating is used in our hybrid optical system based on optical heterodyne scanning system, we performed the correlation of two patterns without using any 2-D SLM at the Fourier plane. Our real-time correlation JTC system enables us to distinguish the difference between two patterns. As we have shown in the theory, if the two patterns are perfectly matched, we expect a strong correlation peak displayed on a real-time display such as an oscilloscope in our case. Based on the theory we have proposed, the optical implementation of the hybrid system is shown. In this system, we employed optical heterodyne scanning with a 1-D chirped grating was used. In comparison to the traditional systems employing SLMs, this system has advantages such as high signal processing speed, simple and robust structure, low cost, also, it does not suffer from the two major drawbacks with the conventional real-time system: the existence of zero-order spectra (because of heterodyning), and the use of a high quality spatial light modulator for coherent display (because of the use of chirp grating). The

effectiveness of this system has been demonstrated by experimental results. This departure from the conventional scheme is extremely important, as the proposed approach does not depend on SLM issues. Consequently, the proposed system should become more acceptable to industry as well as military pattern recognition applications.

In order to strongly confirm our theory and verify our experimental results, computer simulations also have been performed. A MATLAB program has been developed and is shown in Appendix A. The experimental results are in close agreement with the results achieved by computer simulations. We have proposed a novel real-time heterodyne scanning system, which has been successfully realized.

4.2 Future Work

This thesis has developed a novel real-time optical pattern recognition system and experimental results have confirmed the proposed idea. There are some other considerations for future research work, which are s follows:

1. Pattern recognition with vertical position shift, i.e., the two pupils are separated also along the vertical direction.
2. Exploration of multi-object joint-Transform correlation, i.e., there are more than 2 pupils in the front focal plane.

References:

1. T.C Poon and Ron J.Pieper, “novel approach to Real-time Joint Fourier Transform Correlation”, Optics in Comples systems,SPIE Vol.1319,404-405 (1990)
2. . F.T.S.YU and X.J.Lu, “ a real-time programmable joint transform correlator”, Vol. 52, No.1, Optics communications, 10-15, 1 Nov 1984
3. Amit Lal, De Yu Zang, James Millerd, “ laser-diode-based joint transform correlator for fingerprint identification”, Vol.38, No.1, Optical engineering, 69-74, Jan 1989
4. T.Iwaki, Y. Mitsuoka, S.Yamamoto, and H.hoshi, “optical pattern recognition with LAPS-SLM(2)/feedback joint transform correlator using LAPS-SLM.” Vol.1211, SPIE computer and optically formed holographic optics, 284-295, 1990
5. S.A.Ledesma, J.M.Simon, “effect of the aberrations on a joint-transform correlator.” VVol.84, No.1, Optik, 11-16, 1990
6. Shudong Wu, Feng Cheng and Francis T.S.YU, “pattern recognition by OTF method”, vol.20, 5, J.Optics (paris) 201-204. (1989)
7. Joseph Rosen, “three-dimensional optical fourier transform and correlation”, Vol.22, No. 13, Optics Letters, 964-966, July 1, 1997
8. Joseph Rosen and Joseph Shamir, “ Circular harmonic phase filters for efficient rotation-invariant pattern recognition”, Vol. 27, No.14, Applied Optics, 2895-2899,15 July 1988
9. David Casasent and Demetri Psaltis, “ scale invariant optical correlation using mellin transforms”, Vol. 17, No. 1, Optics communications, 59-62, Apr 1976
10. David Casasent and Demetri Psaltis, “ scale invariant optical transform”, Vol. 15, No.3, Optical Engineering, 24-27, May-June 1976
11. Francis T.S.Yu, Feng Cheng, Toshio Nagata, and Don A.Gregory, “effects of fringe binarization of multiobject joint transform correlation”, Vol.28, No.15, Applied Optics, 2988-2990, 1 Aug 1989

12. Thomas Heinrich Barnes, Kiyofumi Matsuda, “joint transform correlator using a phase only spatial light modulator.” Vol. 29, No. 7, Japanese journal of applied physics, 1293-1296, 7, July,1990
13. C.S.Weaver and J.W.Goodman, “A technique for optically convolving two functions,” Appl.Opt.5,B 1248-1249, 1966.
14. G. Lu, Z. Zhang, S. Wu, and F. T. S. Yu., " Implementation of a non-zero-order joint-transform correlator by use of phase-shifting techniques," Appl. Opt. 38, 470-483(1995)
15. Guy Indebetouw and Ting-Chung Poon, “incoherent spatial filtering with a scanning heterodyne system.” Vol. 23, No. 24, Applied Optics, 4571-4574, 15, Dec, 1984
16. David Weber, James Trolinger, “novel implementation of nolinear joint transform correlators in optical security and validation”, Vol.38, No. 1, Optical Engineering, 62-68, Jan, 1999
17. G.Indebetouw, “scanning optical correlator”, Vol.6, NO.1, Optics Letters, 10-12, Jan, 1981
18. B.H.Soffer, G.J.Dunning, Y. Owechko, and E.Marom, “associative holographic memory with feedback using phase-conjugate mirrors”, Vol.11, No. 2, Optics Letters, 118-120, Feb 1986
19. James E,Tanu, “real-time complex spatial modulation”, Vol. 57, No. 6, Journal of the optical society of America, 798-802, June 1967
20. Thomas J. Grycewicz, “applying time modulation to the joint transform correlator”, Vol.33, No. 6, Optical Engineering, 1813-1819, June 1994
21. Francis T.S.Yu, Suganda Jutamulia, Tsongneng W.lin, and Don A.Gregory, “adaptive real-time pattern recognition using a liquid crystal TV based joint transform correlator”, Vol.26, NO. 8, Applied Optics, 1370-1372, 15 Apr 1987
22. Joseph W.Goodman, “Introuduction to Fourier optics”, Mcgraw-Hill, 1968
23. James M. Florence, “joint-transform correlator systems using deformable-mirror spatial light modulators”, Optical society of America, 1989
24. T.C.Poon and A.Korpel, “optical transfer function of an acousto-optic heterodyning image processor”, Vol. 4, No. 10, Optics Letters, 317-319, Oct 1979

25. Ting-Chung Poon, “method of two-dimensional bipolar incoherent image processing by acousto-optic two-pupil synthesis”, Vol 10, No. 5, Optics Letters, 197-199, May 1985
26. A. Korpel, " Acousto-Optics," in Applied Solid State Science, R. Wolfe, ed., Vol.3, Academic, New York (1972).
27. Ting-Chung Poon and Taegeum Kum, “optical image recognition of three-dimensional objects”, Vol.38, No.2, Applied Optics, 370-381, 10 Jan 1999
28. F.T.S.Yu, S.Jutamulia, X.Li and E.Tam, “rotationally invariant joint transform correlation”, Vol.
29. T.-C. Poon and P.P.Banerjee, , Elsevier Science, Contemporary Optical Image Processing With Matlab, Oxford, U.K. , 2001

VITA

Ying QI was born in Liaoning, China in November 1975. She attended the Liaoning University for four years and received a B.S on Physics in 1998.
In 2001, She became a master student in Dep. of Electrical Engineering at Virginia Polytechnic Institute and State University. She pursued his studies and research in the area of optical imaging process in OIP Lab. under the director of Dr. Ting-Chung Poon.